Lund University

Master Thesis

Enhancement of Steady-State Entanglement via Continuous Feedback Control

Author:
Giovanni Francesco Diotallevi

Supervisor:
Peter Samuelsson

Co-supervisors:
Björn Annby-Andersson
Parnam Bakhshinezhad

Thesis submitted for the degree of Master of Science.

Duration: 9 months at 100%

Department of Physics

Division of Mathematical Physics

May 11th, 2023

Acknowledgments

I would like to express my deepest gratitude to my supervisor Peter Samuelsson, who kindly took me in his research group and guided me along the path of research that led to this thesis. Without his ability to deconstruct problems and intuition, this project would have turned out to be much different than what it is now. I would also like to thank my co-supervisors Björn Annby-Andersson and Parnam Bakhshinezhad. Björn's unwavering dedication and pedagogical approach have had a profound impact on my understading of the treated subject. To him, I also owe for having provided the instructive feedback that shaped the quality and direction of the current thesis. On the other hand, I would like to thank Parnam for the support he is been giving me well before the start of this thesis. In the past three years, Parnam took on the role of a mentor to me. To him I owe my gratitude for believing in my past projects and ever so calmly speak his mind regarding my naive approaches in writing and in tackling problems.

In addition, I would also like to thank Armin Tavakoli for the extremely instructive talks and discussions we had over the past months. To him I owe my gratitude for having provided me with new ways to look at the problems presented in this thesis. Together with his, the exchanges of ideas among my office mates represented a great opportunity for me to learn new ideas and obtain new perspectives on my own project. For this I would like to thank Emil Östberg, Daniel Elgbro and Zakaria Mohamed. Laslty, I would like to thank my parents and family, without whose support and encouragement I would have never embarked in the journey that led me to this moment. To them, I dedicate this thesis.

Abstract

Quantum entanglement is a crucial component for many applications in quantum technology. In recent years it has therefore become of great interest to develop methods for generating, controlling and storing entanglement. In 2015, it was shown that a two-qubit engine could generate stationary entanglement exploiting the incoherent interactions with its environment [1]. However, the entanglement generated in such engines is relatively low, and cannot be used for non-classical tasks such as quantum teleportation. In this thesis, we characterize a time-continuous measurement and feedback protocol able to increase the stationary entanglement production in the two-qubit machine. The obtained results show that the developed protocol generates entanglement increments up to seven times higher than those achieved without it. In addition, we show that the entanglement generated through the protocol becomes useful in performing non-classical tasks such as quantum teleportation.

Contents

1 Introduction

Quantum mechanics is a field of physics that tries to address discrepancies between the predictions of classical physics and the observations of systems on an atomic and subatomic scale. At these scales, the equations used to describe otherwise macroscopic systems turn out to be approximations to the laws that quantum mechanics tries to describe. These laws indicate a departure from the traditional understanding of the universe provided by classical mechanics. For instance, quantum mechanics introduces the idea of superposition, through which systems can simultaneously exist in multiple states. This concept departs from the idea of realism and the classical understanding of systems being in a definite state at all times. Another key feature separating classical from quantum physics is entanglement; namely the ability of quantum systems to portray higher levels of correlations than is possible to describe through the formalism of classical physics [2, 3]. In quantum mechanics, the existence of entangled systems establishes a dependency on two measurements even when separated by great distances. This effect challenges the classical notion of locality. For several years, discussions behind the discrepancies between quantum and classical theories remained a topic of debate. However, with an ever increasing understanding of quantum mechanics, in recent years several experiments have supported the claims made by quantum mechanics. In addition, through the development of John S. Bell's inequality formalism, it has been largely established that no successful theory of the universe could simultaneously preserve the ideas of realism and locality.

In recent years, the study of entanglement has seen an increasing amount of interest. This renewed interest emerges from the possibility of using entanglement as a resource. As such, entanglement enables a wide range of applications within the fields of quantum technology and quantum information [4, 5]. Among these, the possibility of using entanglement in quantum computation schemes is of great interest, as it allows for the development of algorithms that are capable of performing meaningful computations that would take far too long for a classical computer to perform [6, 7]. In addition, quantum entanglement has been long established to be a form of thermodynamic resource, thereby allowing it to be used to perform operations in quantum systems such as quantum batteries [8, 9]. Therefore, the generation, storage, and control of entanglement have become central challenges in various areas of quantum physics. Among these, preserving entanglement is a critical challenge in quantum information processing, as the coupling of entangled systems with external environments can quickly degrade the established correlations within the system [10, 11]. One way this challenge can be addressed is through the development of feedback control algorithms. Quantum feedback control is a branch of control theory that aims to control a quantum system through the use of "closed-loop" processes. In a general feedback control setting, a controller monitors some property (observable) of a system. The controller then uses, in real time, the obtained signal to control the dynamics of the measured system. Via means of this general feedback description, several feedback control implementations, formalisms and protocols have been proposed in order to aid the entanglement storage of quantum systems [12–14].

However, it is sometimes possible to exploit dissipative interactions to produce entanglement in the absence of measurement and feedback [15–17]. In Refs. [1, 18], a two-qubit system is capable of generating entanglement exploiting the coherent interaction between the qubits and some external environment. Outside of thermal equilibrium, it is thus possible to show

that these systems are capable of generating long lasting steady state entanglement. The simplicity of these engines allows for the prospect of experimental implementations, however, the entanglement generation capabilities of these engines are limited, and they are often not capable of producing any practically useful amount of entanglement.

In recent years, the study of autonomous thermal engines has seen increased interest as they allow for the investigation of concepts such as work and heat in quantum systems. Experimental implementation of such engines has already been achieved with trapped ions [19,20], while several others have been proposed [21–23]. The engines studied in Refs. [1,18] were first proposed in Ref. [24], and represent the smallest possible form of an autonomous heat engine. The engines are autonomous as they do not require any source of external work to function. In these engines, two qubits are coupled to two thermal resevoirs of different temperature. The two qubits are then left to interact, and the temperature gradient between the two baths establishes a heat current within the two qubit system. Through this scheme, the qubits are capable of extracting useful work, as well as generating weak amounts of entanglement.

In this thesis we address the weakness of the entanglement generated in these engines by developing a continuous feedback protocol. To this end, we define a control parameter for the coupling between the hot bath and the system, which decouples the two whenever an excitation is measured within the system. Via means of this simple procedure, we are able to enhance the entanglement generation of the engines presented in Refs. [1,18]. In addition, we establish a direct relation between the heat currents from the hot bath and the entanglement generated. Lastly, we study the presented protocol under external dephasing and imperfect bath isolation.

2 Theory

In this section we provide the theory required to understand the results presented in chapter 4. We start with a general introduction of quantum systems. Here we introduce the formalism of density operators, their role in quantum mechanics and how to describe their dynamics. We then introduce the basics of entanglement, and discuss how it can be quantified. Lastly, we provide an overview of measurements in quantum mechanics, and the theory behind continuous feedback control.

2.1 Description of Quantum Systems

In the Schrödinger picture of quantum mechanics, quantum systems are represented by time-dependent, normalized statevectors (also known as kets) $|\phi(t)\rangle$ in some complex vector space $\mathcal{H}$. Such a representation is postulated to contain all information regarding the physical state of the system [11, 25]. In addition, it is postulated that for every ket $|\phi\rangle$ there exists a corresponding "bra" $\langle\phi|$, such that $\langle\phi|\phi\rangle = 1$ (normalization condition). In this picture physical observables are represented by linear operators acting on $\mathcal{H}$. The expectation value of any observable $\hat{A}$, with respect to an arbitrary state $|\phi\rangle$, is then defined as

$$\langle\hat{A}\rangle \equiv \langle\phi|\hat{A}|\phi\rangle. \tag{1}$$

When the whole system $|\phi(t)\rangle$ can be considered decoupled from any external system (closed), its time evolution is characterized by the Schrödinger equation (note: $\hbar \equiv 1$)

$$i\partial_t|\phi(t)\rangle = \hat{H}|\phi(t)\rangle, \tag{2}$$

where $\hat{H}(t)$ is the system's Hamiltonian. By solving Eq. (2) for a time independent Hamiltonian, we arrive at an equivalent description for the evolution of $|\phi(t)\rangle$ in terms of a unitary operation denoted by $\hat{\mathcal{U}}(t, t_0)$

$$|\psi(t)\rangle = \hat{\mathcal{U}}(t, t_0)|\psi(t_0)\rangle. \tag{3}$$

where $|\phi(t_0)\rangle$ is system's initial state and $\hat{\mathcal{U}}(t, t_0) = e^{-i\hat{H}(t-t_0)}$ is the time evolution operator which satisfies $\hat{\mathcal{U}}\hat{\mathcal{U}}^\dagger = \hat{\mathcal{U}}^\dagger\hat{\mathcal{U}} = \mathbb{1}$.

For a composite quantum system made up of N different subsystems with complex vector spaces $\mathcal{H}_1, \mathcal{H}_2, ..., \mathcal{H}_N$, the total complex vector space is defined as $\mathcal{H} \equiv \mathcal{H}_1 \otimes \mathcal{H}_2 \otimes ... \otimes \mathcal{H}_N$. Each sub-space has a basis $\{|\phi_j^{(k)}\rangle\}_k$ such that the basis of $\mathcal{H}$ reads $\{|\phi_{j_1}^1\rangle \otimes |\phi_{j_2}^2\rangle \otimes ... \otimes |\phi_{j_N}^N\rangle\}$. Any state in $\mathcal{H}$ may thus be written as

$$|\psi\rangle \equiv \sum_{\phi_1,\phi_2,...,\phi_N} c_{\phi_1,\phi_2,...,\phi_N}|\phi_1\rangle \otimes |\phi_2\rangle \otimes ... \otimes |\phi_N\rangle \tag{4}$$

$$= \sum_{\phi_1,\phi_2,...,\phi_N} c_{\phi_1,\phi_2,...,\phi_N}|\phi_1, \phi_2, ..., \phi_N\rangle, \tag{5}$$

where $c_{\phi_1,\phi_2,...,\phi_N}$ are complex numbers ensuring the normalization condition $\sum_{\phi_1,\phi_2,...,\phi_N} |c_{\phi_1,\phi_2,...,\phi_N}|^2 = 1$.

The state vector formalism discussed so far provides the description of an idealized scenario in which a system can be represented as a pure state vector. However, in experimental settings, due to imperfections in the lab equipment, it is usually not possible to prepare an ensemble of particles to be exactly in some desired state. It is therefore useful to introduce the notion of mixed states, described by density operators $\hat{\varrho}$. A mixed state is characterized by a collection of systems which are prepared with different probabilities p_i, where $\sum_i p_i = 1$. In these cases, a well defined state vector representation $|\phi\rangle$ for the whole system does not exist. Instead, it is useful to define a density operator $\hat{\varrho} \in \mathcal{H}$ as

$$\hat{\varrho} \equiv \sum_i p_i |\phi_i\rangle\langle\phi_i|. \tag{6}$$

Given some orthonormal basis $\{|\phi_i\rangle : i = 1, 2, ..., \dim\mathcal{H}\}$, any density operator can be written in matrix form with elements $\hat{\varrho}_{ij} \equiv \langle\phi_i|\hat{\varrho}|\phi_j\rangle$. In this representation, the diagonal elements $\hat{\varrho}_{ii}$ represent populations and give the probability for the system to be in state $|\phi_i\rangle$, while the off-diagonal elements $\hat{\varrho}_{ij}$ $(i \neq j)$ are referred to as coherences and indicate the presence of superposition of the basis-states within the system. Because of this, we formulate a normalization condition for all density operators, namely

$$\mathrm{Tr}\{\hat{\varrho}\} = 1. \tag{7}$$

Due to the properties of the trace operation, the holds true for any choice of basis we decide to represent $\hat{\varrho}$ in. In addition, we see that $\hat{\varrho}$ needs to be positive and Hermitian (i.e. $\langle\phi_i|\hat{\varrho}|\phi_i\rangle \geq 0$ and $\hat{\varrho}^\dagger = \hat{\varrho}$, for any $\{|\phi_i\rangle\}$).

Equation (6) shows that density operators are a generalization of state vectors, as any pure state vector can be represented through as a density operator, while the converse is not always true. To distinguish the cases in which a density operator $\hat{\varrho}$ can be fully described by a state vector, we introduce the notion of purity $0 \leq P(\hat{\varrho}) \leq 1$. According to this parameter, all pure states are characterized by $P(\hat{\varrho}) = 1$, in these cases there exist a pure state $|\phi\rangle$ such that $\hat{\varrho} = |\phi\rangle\langle\phi|$. Given any density operator $\hat{\varrho}$, the purity of the system is defined as

$$P(\hat{\varrho}) \equiv \mathrm{Tr}\left\{\hat{\varrho}^2\right\}. \tag{8}$$

For systems of unit purity, the expectation value for a given observable $\hat{A}$ is given by Eq. (1). Although, for systems with $P(\hat{\varrho}) < 1$ there exist no pure state vector representation and Eq. (1) does not hold anymore. In these cases, the expectation value of some observable $\hat{A}$ can be shown to take the form

$$\langle\hat{A}\rangle \equiv \mathrm{Tr}\left\{\hat{A}\hat{\varrho}\right\}. \tag{9}$$

The time evolution of closed mixed ensembles can also be treated through the formalism of unitary evolutions (see Eq. (3)). Consider a quantum statistical ensemble characterized by a density operator of the form $\hat{\varrho}(t_0) = \sum_i p_i |\phi_i(t_0)\rangle\langle\phi_i(t_0)|$. Using Eq. (3), we see that the time evolved state for $\hat{\varrho}$ is $\hat{\varrho}(t) = \hat{\mathcal{U}}(t, t_0)\hat{\varrho}(t_0)\hat{\mathcal{U}}^\dagger(t, t_0)$. Differentiating this equation gives the Liouville-von Neumann equation

$$\frac{d}{dt}\hat{\varrho}(t) = i\left[\hat{\varrho}(t), \hat{H}\right]. \tag{10}$$

Assume we had a composite quantum system (here we focus on bipartite systems for simplicity),described by a density matrix $\hat{\varrho}_{\mathrm{SE}}$. It is useful to define a reduced state for sub-system S, by introducing the partial trace operation

$$\hat{\varrho}_{\mathrm{S}} = \mathrm{Tr}_{\mathrm{E}}\left\{\hat{\varrho}_{\mathrm{SE}}\right\} = \sum_i \langle \phi_i^{\mathrm{E}} | \hat{\varrho}_{\mathrm{SE}} | \phi_i^{\mathrm{E}} \rangle, \tag{11}$$

where $\{|\phi_i^{\mathrm{E}}\rangle\}$ are the basis states for sub-system E. Equation (10) is valid only until the mixture does not interact with some external environment. If we wished to study the dynamics of a mixture $\hat{\varrho}_{\mathrm{S}} \in \mathcal{H}_{\mathrm{S}}$ coupled to some external environment $\hat{\varrho}_{\mathrm{E}} \in \mathcal{H}_{\mathrm{E}}$, Eq. (10) would still hold if we considered the evolution of the closed product state $\hat{\varrho}_{\mathrm{SE}} = \hat{\varrho}_{\mathrm{S}} \otimes \hat{\varrho}_{\mathrm{E}}$ between system and environment. In principle, after evolving the product state according to Eq. (10), one can find the final state of $\hat{\varrho}_{\mathrm{S}}$ via means of Eq. (11) such that

$$\hat{\varrho}_{\mathrm{S}}(t) = \mathrm{Tr}_{\mathrm{E}}\left\{\hat{\mathcal{U}}(t,t_0)\hat{\varrho}_{\mathrm{SE}}(t_0)\hat{\mathcal{U}}^{\dagger}(t,t_0)\right\}. \tag{12}$$

Although Eq. (12) is an exact dynamical equation, analytically solving this equation is often challenging. There are several possible models that can be used to approximate Eq. (12). Among these approximate methods, one can derive a Markovian master equation known as the "Lindblad master equation" for the evolution of a system $\hat{\varrho}_{\mathrm{S}}$ coupled to one or more environments [10, 26]

$$\partial_t \hat{\varrho}_{\mathrm{S}} \equiv \mathcal{L}\hat{\varrho}_{\mathrm{S}} = i\left[\hat{\varrho}_{\mathrm{S}}, \hat{H}\right] + \sum_k \Gamma_k \left(\hat{J}_k \hat{\varrho}_{\mathrm{S}} \hat{J}_k^{\dagger} - \frac{1}{2}\left\{\hat{J}_k^{\dagger}\hat{J}_k, \hat{\varrho}_{\mathrm{S}}\right\}\right) \tag{13}$$

$$= i\left[\hat{\varrho}_{\mathrm{S}}, \hat{H}\right] + \sum_k \Gamma_k \mathcal{D}[\hat{J}_k]\hat{\varrho}_{\mathrm{S}}, \tag{14}$$

where we have introduced $\mathcal{L}$ as the Lindblad superoperator describing the time evolution of $\hat{\varrho}$ and the dissipator superoperators $\mathcal{D}[\hat{\Omega}]\hat{\varrho} \equiv \hat{\Omega}\hat{\varrho}\hat{\Omega}^{\dagger} - \frac{1}{2}\left\{\hat{\Omega}^{\dagger}\hat{\Omega}, \hat{\varrho}\right\}$ for any operator $\hat{\Omega}$. In Eq. (14) the operators $\hat{J}_k$ are usually referred to as Lindblad operators and typically describe particle and energy exchanges with the environment, while Γ_k characterize the rate at which these exchanges occur. For example, consider a one qubit system coupled to a single environment k. Using the $\{|0\rangle, |1\rangle\}$ computational basis, the Lindblad operator is written as $\hat{J}_k = |1\rangle\langle 0|$, which describes the excitation event of the qubit due to the interaction with its environment. The validity of Eq. (14) is established by a weak coupling strength between $\hat{\varrho}_{\mathrm{S}}$ and its environment, and by the correlations between system and bath remaining negligible over time [1, 10, 26].

2.2 Entanglement

In this thesis we focus on bipartite entanglement, but note that multipartite entanglement also exists. Physicists often refer to uncorrelated quantum systems as separable. This is because two uncorrelated pure quantum systems with state vectors $|\phi_{\mathrm{A}}\rangle$ and $|\phi_{\mathrm{B}}\rangle$ can be described as a single product state $|\phi_{\mathrm{AB}}\rangle = |\phi_{\mathrm{A}}\rangle \otimes |\phi_{\mathrm{B}}\rangle$ (see Eq. (5)). For such a system, the two subsystems are independent, and any interaction with either system will leave our

knowledge about the other unchanged. A pure state that cannot be written like this is said to be entangled. More rigorously, the bipartite systems considered in this thesis live in the complex vector space $\mathcal{H} = \mathcal{H}_1 \otimes \mathcal{H}_2$, where $\dim\mathcal{H}_1 = \dim\mathcal{H}_2 = 2$. Using the computational basis $\{|0\rangle, |1\rangle\}$, this vector space can be shown to be spanned by the four maximally entangled Bell state basis

$$|\Psi_\pm\rangle = \frac{1}{\sqrt{2}}(|01\rangle \pm |10\rangle), \qquad |\Phi_\pm\rangle = \frac{1}{\sqrt{2}}(|00\rangle \pm |11\rangle). \tag{15}$$

Figure (1) shows an illustration of the corresponding density operator for two of the four states in Eq. (15): the height of each bar indicates the absolute value of the corresponding element in the matrix, while the color of each bar provides information about their complex phase. A remarkable feature of the states in Eq. (15) arises upon measuring the state of either one of the particles comprising the whole system. Upon doing so, one recovers the state of this particle to be either $|0\rangle$ or $|1\rangle$ with 50% probability. Although, being the whole system in a pure state, the act of measuring a single particle allows for the complete characterization of the total state, thus affecting the measurement outcome on the second system, regardless of the distance between the two.

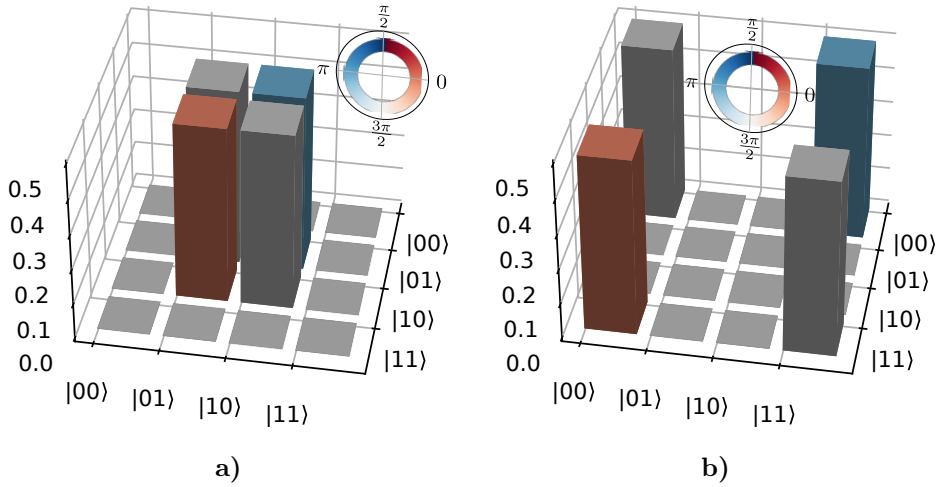

Figure 1: Elements of two density operators constructed using two of the four maximally entangled Bell-states (see Eq. (15)). The bar height indicates the absolute value of the corresponding element, while the color encodes the complex phase of each element. The pure states whose density matrix we are showing here are: **a)** $|\Psi_-\rangle = \frac{1}{\sqrt{2}}(|01\rangle - |10\rangle)$, **b)** $|\Phi_-\rangle = \frac{1}{\sqrt{2}}(|00\rangle - |11\rangle)$.

On the other hand, mixed entangled states are defined as those that cannot be written as $\hat{\varrho}_{\mathrm{AB}} = \sum_j p_j \hat{\varrho}^j_{\mathrm{A}} \otimes \hat{\varrho}^j_{\mathrm{B}}$ [2], where p_j are positive constants ensuring the normalization condition in Eq. (7). This definition of entanglement suggests a binary classification between entangled and non entangled states. For instance, for mixed state entanglement, this definition does not provide any insight of how much entangled, or how useful a given state is for quantum information processes. As an example, we can consider the mixed state $\hat{\varrho}_{\mathrm{AB}} = p|\Psi_+\rangle\langle\Psi_+| + (1-p)|00\rangle\langle 00|$, with $0 \leq p \leq 1$. For $p \to 0$, the state becomes fully separable, while it is maximally entangled when $p \to 1$. It is thus not clear how useful the entanglement is for small values of p. To resolve such issues, several measures have been introduced, attempting

to quantify the amount of entanglement of a given state [27–29]. Such measures have been postulated as to satisfy a number of conditions; here we discuss the most commonly used conditions. Firstly, for any entanglement measure E of a given state $\hat{\varrho}$ we have $0 \leq E(\hat{\varrho}) \leq 1$, where $E(\hat{\varrho}) > 0$ for any entangled state. Moreover, $E(\hat{\varrho}) = 0$ for separable states, while $E(\hat{\varrho}) = 1$ for any of the Bell-states. Lastly, entanglement measures are defined as monotonic state quantities under any local operation and classical communication (LOCC) $\Lambda(\hat{\varrho})$ [2, 27]

$$E(\Lambda(\hat{\varrho})) \leq E(\hat{\varrho}). \tag{16}$$

In short, LOCC operations are all operations that can be independently performed on single subsystems of a quantum system and involve only classical communication between the subsystems. As an example one could think of trying to distinguish an entangled state (see Eq. (15)) of two particles shared between two observers (say Alice and Bob). To do so Alice and Bob could use a classical channel, say a telephone line, to compare the results obtained upon separately measuring the state of the respective particles, thus revealing the initial state of the joint system. This is an important property of entanglement measures, as it suggests that the entanglement within a system cannot be increased through local operations alone.

In this thesis we quantify the entanglement content of a given state $\hat{\varrho}$ using the entanglement measure known as concurrence. However, as discussed below in detail, concurrence does not necessarily indicate how useful the entanglement content of $\hat{\varrho}$ is for quantum information processes. To this end, it is instructive to benchmark the ability of $\hat{\varrho}$ in performing non-classical tasks, such as quantum teleportation and violating Bell's inequality, see Secs. 2.2.2 and 2.2.3.

2.2.1 Concurrence

Concurrence is an entanglement measure that tries to quantify the resources needed to produce non-separable states between a pair of two-level systems (i.e. qubits) [30]. The concurrence of a bipartite qubit system state $\hat{\varrho}$ takes the form

$$C(\hat{\varrho}) = \max\{0, \lambda_0 - \lambda_1 - \lambda_2 - \lambda_3\}, \tag{17}$$

where $\{\lambda_i\}$ are the eigenvalues of the Hermitian operator $R = \sqrt{\sqrt{\hat{\varrho}}\hat{\varrho}'\sqrt{\hat{\varrho}}}$, sorted in decreasing order (i.e. $\lambda_3 < \lambda_2 < \lambda_1 < \lambda_0$) and where $\hat{\varrho}' = (\hat{\sigma}_y \otimes \hat{\sigma}_y)\,\hat{\varrho}^*\,(\hat{\sigma}_y \otimes \hat{\sigma}_y)$ is the spin-flipped state, and $\hat{\sigma}_y = i(|1\rangle\langle 0| - |0\rangle\langle 1|)$ is the Pauli-y matrix and $\hat{\varrho}^*$ is the complex conjugate of $\hat{\varrho}$ taken element wise. In this thesis, we focus on systems coupled to external reservoirs. Due to this coupling, most coherences of our systems will vanish, leaving us with states whose density matrix $\hat{\varrho}$ can be written in the form (see chapter 3)

$$\varrho = \mathcal{N}\begin{bmatrix} \varrho_0 & 0 & 0 & 0 \\ 0 & \varrho_1 & \alpha & 0 \\ 0 & \alpha^* & \varrho_2 & 0 \\ 0 & 0 & 0 & \varrho_3 \end{bmatrix}, \tag{18}$$

where $\mathcal{N}$ is a constant ensuring the normalization condition for density matrices. In these cases, the expression for the concurrence of the system assumes the simplified form

$$C(\hat{\varrho}) = \max\left\{2\mathcal{N}\left(|\alpha| - \sqrt{\varrho_0\varrho_3}\right), 0\right\}. \tag{19}$$

Using Eq. (17) to obtain the concurrence of any of the Bell-states and that of any maximally mixed state (i.e. $P(\hat{\varrho}) = 0.25$), we note that this quantifier is successful in classifying maximum entangled states and non-entangled states. However, concurrence is not capable of accounting for all non-classical resources contained in a system. To show this, consider the entangled state $|\phi_p\rangle = \sqrt{p}|01\rangle + \sqrt{1-p}|10\rangle$ for $p \in (0, 1)$. This state is Bell non-local, thus capable of showcasing non-local behaviours for any value of p. However, according to Eq. (19) the concurrence for this state can reach arbitrarily small values $C(|\phi_p\rangle\langle\phi_p|) = 2\sqrt{p-p^2}$. Additionally, there exist a non-ordering theorem that prevents two separate entanglement measures to agree on the entanglement content of different states [31]. This means that, for a general set of states, concurrence will predict a unique ordering based on the amount of entanglement contained in these, while another measure could predict an entirely different ordering. To account for these shortcomings, in our studies we include two additional entanglement quantifiers to asses the performance of a given state in operating purely non-classical tasks, these being quantum teleportation and Bell non-locality.

2.2.2 Teleportation

Quantum teleportation is a quantum communication protocol through which two observers, say Alice and Bob, are allowed to send copies of qubit states to each other. In a general quantum teleportation scheme, teleportation is achieved via means of a classical communication channel and two additional fully entangled qubits, which enable a higher teleportation fidelity that would be achievable classically [32,33]. In a general quantum teleportation protocol, Alice and Bob share a pair of entangled qubits represented by the state $\hat{\varrho}$. Alice then wants to send to Bob a qubit state $|\psi\rangle$. To achieve this, she projects $|\psi\rangle$ and her part of $\hat{\varrho}$ onto the basis of the four maximally entangled states in Eq. (15) and sends the result to Bob via some classical communication channel. Bob then applies a unitary transformation on his side of $\hat{\varrho}$ based on the projection outcome obtained by Alice. At the end of this protocol, if $\hat{\varrho}$ constituted a maximally entangled state, Alice has successfully sent $|\psi\rangle$ to Bob with 100% fidelity. In this thesis, the fidelity of this protocol quantifies the closeness between the state obtained by Bob, and the initial state $|\psi\rangle$.

The focus of this thesis does not rely on the specifics of the algorithm that renders this protocol possible. Rather, we are here interested in the fidelity f for this task given a set of entangled qubits. The fidelity for this protocol takes the form $f = \frac{1+2F}{3}$ [18, 34], where F is defined as the singlet fraction for $\hat{\varrho}$. In general, the singlet fraction for a general state has no closed form. However, for states of the form of Eq. (18) the singlet fraction takes the form [18]

$$F(\hat{\varrho}) = \begin{cases} \alpha + \frac{\Delta}{2} & \text{if} \quad (1 + 2\alpha - 2\Delta) \leq 0 \\ \max\{\alpha + \frac{\Delta}{2}, \frac{1-\Delta}{2}\} & \text{otherwise} \end{cases} \tag{20}$$

where $\Delta = \mathcal{N}(\hat{\varrho}_1 + \hat{\varrho}_2)$ (see Eq. (18)). In the best case, a classical implementation of the protocol can only achieve a fidelity $f = \frac{2}{3}$, thus, for a state portraying purely non classical behaviours, the singlet fraction must lie $F(\hat{\varrho}) > \frac{1}{2}$.

2.2.3 Non-Locality

The last entanglement quantifier studied in this thesis is Bell's inequality. In 1935 Albert Einstein, Boris Podolsky and Nathan Rosen (EPR) published a paper in which they argued for the incompleteness of quantum mechanics [35]. EPR suggested that quantum mechanics was unable of capturing all the variables needed to make definite predictions about the outcome of a measurement. In EPR's view, there should exist hidden variables that a successful theory should be able to account for, thus eliminating the probabilistic nature of quantum mechanics. EPR's argumentation was in part driven by the seemingly non local properties of entangled states, as measuring one part of an entangled system would affect the rest of the system in a seemingly instantaneous way, regardless of distance. The question regarding the completeness of quantum mechanics remained largely unanswered until 1964. In this year, John S. Bell published a paper in which he addressed the concerns raised by EPR. In his paper, John Bell put forward an experimentally verifiable inequality that, if violated, would prove the impossibility of a local realist hidden variable theory [36]. Ever since Bell's publication in 1964, a series of experiments denoted as Bell tests have been performed in order to establish the existence of such hidden variable theories [37–39].

In short, Bell's inequality can be reconstructed via the consideration of a thought experiment. Suppose that a third party (Charlie) is capable of preparing pairs of particles in a controlled way. Once a pair is prepared, Charlie distributes the two particles between two observers, Alice and Bob. Upon receiving their particles, Alice and Bob perform a measurement on their particle, by randomly deciding to measure either one of two properties P_Q and P_R, for Alice, P_T and P_S for Bob. For simplicity, let us assume that the measurements can yield outcomes ± 1. Let us then consider Alice's particle to have value Q for property P_Q and value R for property P_R. Analogously, let us assume Bob's particle to have value S for property P_S and value T for property P_T. Now suppose that $p(s,q,r,t)$ is the probability for the joint system to be such that $S=s$, $Q=q$, $R=r$, $T=t$ before the measurement. Note that the probabilistic nature for the measured properties arises for the necessity of considering Charlie's imperfect preparation, or as a consequence of noisy equipment. Let $\mathbf{E}(x(s,q,r,t)) = \sum_{s,q,r,t} xp(s,q,r,t)$ represent the expectation value of the input quantity x, we then have [11]

$$\mathbf{E}(QS + RS + RT - QT) = \sum_{sqrt} p(s,q,r,t)(qs + rs + rt - qt) \tag{21}$$

$$= \mathbf{E}(QS) + \mathbf{E}(RS) + \mathbf{E}(RT) - \mathbf{E}(QT) \leq 2, \tag{22}$$

where the inequality of Eq. (22) comes about as we have that $QS + RS + RT - QT = \pm 2$.

The inequality presented in Eq. (22) is known as $CHSH$ inequality from the initials of those who first derived it John F. Clauser, Michael A. Horne, Abner Shimony and Richard A. Holt (CHSH) [40]. In this thesis, we study the $CHSH$ of our states to quantify the non-local properties of our results. For states taking the form presented in Eq. (18), the inequality is expressed as [18, 41]

$$\text{CHSH} = 2\sqrt{8\alpha^2 + (2\Delta - 1)^2 - \min\{4\alpha^2, (2\Delta - 1)^2\}} \leq 2, \tag{23}$$

where $\Delta = \mathcal{N}(\hat{\varrho}_1 + \hat{\varrho}_2)$ (see Eq. (18)). From this, we gather that for any state capable of

portraying non-local behaviours, the CHSH must lie above 2, where a maximally entangled state (see Eq. 15) is capable of obtaining at most CHSH $= 2\sqrt{2}$.

2.3 Heat in Open Quantum Systems

In Ref. [1] it was shown that a non-zero heat current is necessary to generate steady state entanglement. Furthermore, in Ref. [42] an expression for a critical heat current required to generate entanglement in the studied thermal engines was derived. It is therefore useful to provide a short discussion of how heat currents are calculated for systems weakly coupled to their environment.

For an open system coupled to several thermal environments of various temperatures, there will be a flow of heat through the system. In general the total energy change of an open system is calculated through Eq. (9) as $\dot{E} = \mathrm{Tr}\left\{\hat{\varrho}\partial_t\hat{H}\right\} + \mathrm{Tr}\left\{\hat{H}\partial_t\hat{\varrho}\right\}$. The engines studied in this thesis are autonomous, and therefore need no external agent to operate. Because of this, the Hamiltonian of the system is time independent, which allows us to simplify the expression for the energy change within the system to $\dot{E} = \mathrm{Tr}\left\{\hat{H}\partial_t\hat{\varrho}\right\}$. The heat flow between the system and bath k is then defined as

$$\dot{Q}_k = \mathrm{Tr}\left\{\left(\hat{H} - \mu_k\hat{N}\right)\mathcal{L}_k\hat{\varrho}\right\}, \tag{24}$$

where $\hat{N}$ is the number operator of particles within the system, μ_k is the chemical potential of bath k ($\mu_k = 0$ for bosonic baths) and $\mathcal{L}_k\hat{\varrho} = \sum_i \Gamma_{k,i}\left(\hat{J}_{k,i}\hat{\varrho}\hat{J}^\dagger_{k,i} - \frac{1}{2}\left\{\hat{J}^\dagger_{k,i}\hat{J}_{k,i}, \hat{\varrho}\right\}\right)$ is the Lindblad superoperator arising from the coupling with bath k [43, 44]. In this thesis we use Eq. (24) to study the relation between the entanglement generation properties of the studied systems and the heat provided by the coupled environments.

2.4 Measurements in Quantum Mechanics

In this section we present the formalism of measurements in quantum mechanics. We begin with a brief introduction of von-Neumann (projective) measurements, as often introduced in early quantum mechanics courses. We then discuss generalized quantum measurements.

2.4.1 von-Neuman Measurements

It is often the case in quantum mechanics that, when speaking about measurements, physicists refer to a special class of measurements called projective measurements (also known as von-Neumann measurements or strong measurements) [11, 45]. Given an observable $\hat{A}$ with eigenstates $\{|\mathrm{a}\rangle : \mathrm{a} = 1, 2, ..., \mathrm{a}_{\max}\}$, the system is projected onto one of the possible eigenstates, and the outcome of the measurement is given by the corresponding eigenvalue. For example, given a state $|\phi\rangle = \sum_\mathrm{a} c_\mathrm{a}|\mathrm{a}\rangle$, a projective measurement on $|\phi\rangle$, would project the system onto state $|\mathrm{a}\rangle$ with probability $|c_\mathrm{a}|^2$. That is, after the measurement we know the state of the system, but the initial state is destroyed.

Note that the repeated use of projective measurements can give rise to a phenomenon known as the quantum Zeno effect [46–48]: this phenomenon freezes systems in one state,

preventing them from evolving any further. The Zeno effect arises as a consequence of the instantaneous destruction of the coherences within the system. To circumvent this problem, we construct a measurement operator with the ability to preserve coherences, but with the added drawback of recovering only partial information from a quantum system.

2.4.2 Generalized Quantum Measurements

We now discuss generalized quantum measurements, describing a much broader class of measurements than von-Neumann measurements. Although projective measurements represent only a subclass of all possible measurements, their formalism can be used to describe a wider variety of measurement operations [25,46]. In this thesis, we use projective measurements to construct operations capable of extracting only partial information about a given observable $\hat{A}$: i.e. weak measurements. As a consequence of the increase in the uncertainty of the measurement outcomes, both the system's dynamics suppression and coherence erasure problem will disappear.

In general, any set of generalized measurement operators $\left\{\hat{M}_z\right\}$ must satisfy the completeness relation

$$\sum_z \hat{M}_z^\dagger \hat{M}_z = \mathbb{1}, \tag{25}$$

which ensures that the probabilities of obtaining any outcome from the measurement operations add to unity. In the scenario of strong measurements, the measurement operators $\left\{\hat{M}_z\right\}$ are represented by projection operators, where z denotes the measurement outcome. A useful example is the measurement of a qubit in the computational $\{|0\rangle, |1\rangle\}$ basis, where $\hat{M}_0 = |0\rangle\langle 0|$ and $\hat{M}_1 = |1\rangle\langle 1|$. Formally, the third postulates of quantum mechanics states that measuring $\hat{\varrho} = \sum_i p_i |\phi_i\rangle\langle\phi_i|$ with a measurement operator $\hat{M}_z$ updates the system as [11]

$$\hat{\varrho}_z = \sum_i p_i \frac{\hat{M}_z|\phi_i\rangle}{\sqrt{\langle\phi_i|\hat{M}_z^\dagger \hat{M}_z|\phi_i\rangle}} \frac{\langle\phi_i|\hat{M}_z^\dagger}{\sqrt{\langle\phi_i|\hat{M}_z^\dagger \hat{M}_z|\phi_i\rangle}} \tag{26}$$

$$= \frac{\hat{M}_z \hat{\varrho} \hat{M}_z^\dagger}{\mathrm{Tr}\left\{\hat{M}_z^\dagger \hat{M}_z \hat{\varrho}\right\}}, \tag{27}$$

where $\hat{\varrho}_z$ is the updated state conditioned on the outcome z (see appendix C for a discussion on conditional and non-selective states), while $p_z = \mathrm{Tr}\left\{\hat{M}_z^\dagger \hat{M}_z \hat{\varrho}\right\}$ represents the probability of obtaining outcome z and ensures the normalization condition of Eq. (7). In contrast to the description provided in Sec. 2.1, the update Eq. (27) is non-linear in $\hat{\varrho}$ and leads to non-unitary dynamics. This can be understood as a consequence of introducing a measuring apparatus in the form of an external environment which renders Eq. (10) no longer true.

We now study a special class of measurement operators known as Gaussian measurements. Given an observable $\hat{A}$ with eigenstates $\{|\mathrm{a}\rangle : \mathrm{a} = 1, 2, ..., \mathrm{a}_{\max}\}$ and eigenvalues $\{\mathrm{a} : \mathrm{a} = 1, 2, ..., \mathrm{a}_{\max}\}$, we define a measurement operator $\hat{W}(z)$ as the gaussian weighted sum of

projections onto the eigenstates of $\hat{A}$

$$\hat{W}(z) \equiv \left(\frac{2\kappa}{\pi}\right)^{\frac{1}{4}} e^{-\kappa\left(z-\hat{A}\right)^2}, \tag{28}$$

where κ is a standard deviation related parameter and z is a continuous variable labelling the possible measurement outcomes. In principle, we could have defined a measurement operation weighted with some other function. However, the choice of using Gaussian measurements stems from the popularity of these within experimental settings. Given the definition in Eq. (28), the only condition that $\hat{W}(z)$ has to satisfy, is therefore the completeness relation (see Eq. (25)) $\int_{-\infty}^{\infty} \hat{W}^\dagger(z)\hat{W}(z)dz = 1$ [11, 25] (for proof of completness refer to appendix A).

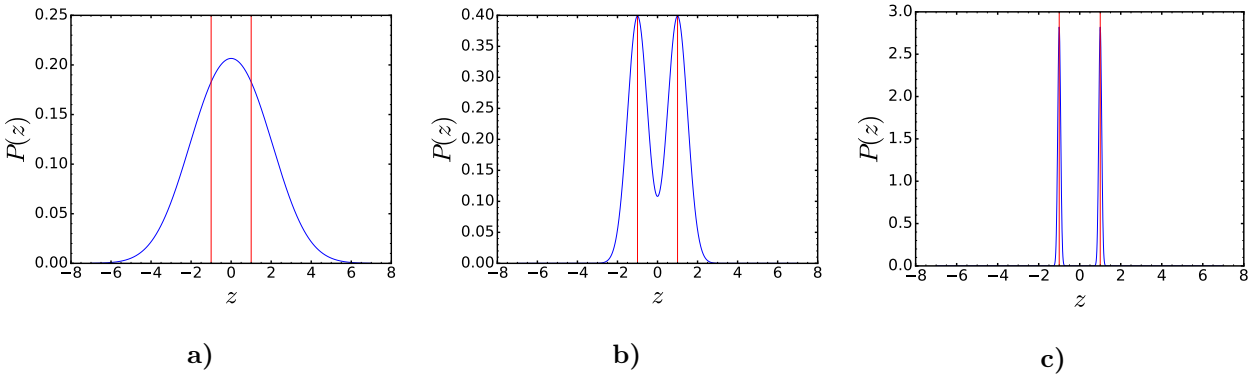

Figure 2: Graphs illustrating the probability distribution for results obtainable through a weak measurement of a single qubit (here $\hat{A} = \hat{\sigma}_z$). The leftmost figure shows the probability distribution in the weak regime (i.e. $\kappa \to 0$); the rightmost figure shows the same distribution, in a strong measurement regime (i.e. $\kappa \to \infty$); the center figure shows the probability distribution for an intermediate measurement strength. The vertical red lines are positioned at $z = -1$ and $z = 1$ for reference.

From Eq. (28), we see that $\hat{W}(z)$ represents a superposition of gaussian curves centered at the possible measurement outcomes z. Additionally, as $\kappa \to \infty$, $\hat{W}(z)$ approaches the definition of a δ-function centered at z (projective limit); thus, we define κ as the measurement strength parameter. Figure 2 illustrates the effect of κ on the probability distribution $P(z)$ for measuring outcome z for a qubit initialized in a maximally mixed state (i.e. $\hat{\varrho} = \frac{1}{2}(|0\rangle\langle 0| + |1\rangle\langle 1|)$ in the $\{|0\rangle, |1\rangle\}$ computational basis). From Fig. 2, we see that as $\kappa \to \infty$ the probability distribution narrows to the two possible outcomes $z = \pm 1$ (i.e. projective limit).

2.4.3 Continuous Measurements

Above we discussed the scenario where a single measurement is performed. In many setups, such as semiconductor quantum dots, it is common to perform time continuous measurements [49–51]. For our purposes, these measurements cannot be projective. If they were, the coherence of the system would quickly vanish. Instead, we need to perform weak measurements in a continuous fashion, in order to preserve the coherences within the system. In this section we construct a formalism for measurement operations capable of extracting information in a continuous way. To avoid the quantum Zeno effect, it is necessary that each

measurement becomes infinitely weak, we thus set $\kappa = \lambda dt$, such that $\kappa \to 0$ as $dt \to 0$ [25,52]. We then use Eq. (28) to define a continuous measurement operator $\hat{K}(z)$ as

$$\hat{K}(z) \equiv \left(\frac{2\lambda dt}{\pi}\right)^{\frac{1}{4}} e^{-\lambda dt\left(z-\hat{A}\right)^2}. \tag{29}$$

Through a similar analysis as the one conducted when presenting Eq. (28), we see that as $dt \to 0$, the width of $\hat{K}(z)$ varies as $1/dt^{1/2}$: thus, the lower dt, the more uncertainty in the measurement outcome. Notice that, given a fixed dt, it is now λ that defines the measurement strength. The measurement outcome z is then modelled as a stochastic variable as a result of the stochastic nature of measurements in quantum mechanics [25, 52], which we write as

$$z = \langle \hat{A} \rangle + \frac{\Delta W}{(8\kappa)^{1/2}\,\Delta t}, \tag{30}$$

where ΔW is a normal distributed random white-noise variable with zero-mean. Thus, we also require ΔW to be uncorrelated with itself at different times, i.e. $\langle \Delta W(t_1)\Delta W(t_2)\rangle = \delta_{t_1 t_2}$, where $\delta_{t_1 t_2}$ is the Kronecker delta function in discrete processes or the Dirac delta function in a continuous limit.

With Eq. (29), we have derived the form of an operator capable of characterizing the measurement backaction effects onto the measured system. In theory, it is then possible to model a continuously monitored system by having $dt \to 0$. In this limit, the evolution of a continuously monitored conditional state is designed as

$$\hat{\varrho}_{t_f}(\overline{z}) = e^{\mathcal{L}dt}\mathscr{M}(z_n)...e^{\mathcal{L}dt}\mathscr{M}(z_1)\hat{\varrho}_0, \tag{31}$$

where we have defined the superoperator $\mathscr{M}(z)\hat{\varrho}_t = \frac{\hat{K}(z)\hat{\varrho}\hat{K}^\dagger(z)}{\mathrm{Tr}\left\{\hat{K}^\dagger(z)\hat{K}(z)\hat{\varrho}\right\}}$, while $\mathcal{L}$ represents the free evolution Lindblad superoperator found in Eq. (14). In appendix D, we make use of Eq. (31) to derive an expression for the evolution of a continuously monitored non-selective state, otherwise evolving according to Eq. (14). There, we find

$$\partial_t \hat{\varrho}_t = \mathcal{L}\hat{\varrho}_t + \lambda\mathcal{D}[\hat{A}]\hat{\varrho}_t. \tag{32}$$

Compared to Eq. (14), Eq. (32) contains an additional dissipator term describing how the system is dephased in the observalble $\hat{A}$'s eigenbasis.

2.5 Feedback

In this section we introduce the formalism of continuous feedback control. In general, continuous feedback is implemented by

$$\hat{\varrho}_{t+dt}(D) = e^{\mathcal{L}(D)dt}\mathscr{M}(z)\hat{\varrho}_t, \tag{33}$$

where $\mathscr{M}(z)\hat{\varrho}_t = \frac{\hat{K}(z)\hat{\varrho}\hat{K}^\dagger(z)}{\mathrm{Tr}\left\{\hat{K}^\dagger(z)\hat{K}(z)\hat{\varrho}\right\}}$ represents the measurement action, while $\mathcal{L}(D)$ represents the feedback controlled dynamics of the system, with $\mathcal{L}(D)$ written in Lindblad form (see

Eq. (14)) and the filtered measurement outcome D being defined as (see appendix E for additional details)

$$D(t) = D(t_0)e^{-\gamma(t-t_0)} + \gamma \int_{t_0}^{t} e^{\gamma(s-t)} z(s) ds, \tag{34}$$

where γ represents the bandwidth of the detector, which characterizes the detector's response rate as $1/\gamma$ and where $D(t_0)$ represents the filtered measurement outcome obtained at the initial time t_0. The definition of Eq. (34) can be seen as a convollution of the measurement outcomes z with some lorentzian function in Fourier-space, thus it represents a general filtering process valid independently from the choice of observable $\hat{A}$.

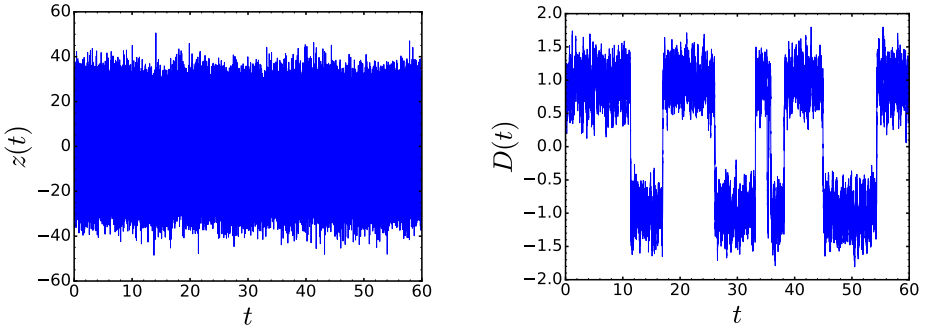

a) **b)**

Figure 3: Results obtained from a quantum Monte Carlo simulation for a qubit system (initiated in $|10\rangle\langle 10|$). The left most graph represents the measurement outcome z over time (see Eq. (30)). We see that the variance for z becomes far too great in the continuous limit, and no useful information can be extracted. The right most graph shows the filtered measurement outcomes. We see that the chosen filtering method is capable of returning useful information that can be used in the feedback protocol.

In Fig. 3, we illustrate the effect of the detector's bandwidth, by numerically evolving a qubit system initiated in $|10\rangle\langle 10|$ through a Monte Carlo simulation. In Fig. 3.a, the signal $z(t)$ is generated in the detector with a white noise distribution in accordance with Eq. (30). The circuitry of the detector filters out the the high frequency noise according to Eq. (34), and we read off $D(t)$ (see Fig. 3.b).

2.5.1 Quantum Fokker-Planck Master Equation

It is in general the case that, when dealing with continuous measurement and feedback protocols, the system state is either numerically evolved according to stochastic differential equations (see Eq. (33)), or otherwise analytically evolved according to Markovian master equations which are limited to a linear dependence in the measured signal [53]. An exception to this comes from a recent development in the theoretical description of feedback control [54], in which a quantum Fokker-Planck master equation (QFPME) for continuous feedback control was derived. In short, this formulation can be obtained by averaging Eq. (33) over all possible outcomes $D(t)$, but leaving the last outcome D fixed. This procedure then gives

$$\partial_t \hat{\varrho}_t(D) = \mathcal{L}(D)\hat{\varrho}_t(D) + \lambda \mathcal{D}[\hat{A}]\hat{\varrho}_t(D) - \gamma \partial_D \mathcal{A}(D)\hat{\varrho}_t(D) + \frac{\gamma^2}{8\lambda}\partial_D^2 \hat{\varrho}_t(D). \tag{35}$$

The density operator $\hat{\varrho}(D)$ is then defined as the joint system-detector state, where the non-selective system representation is given by $\hat{\varrho}_t = \int dD \hat{\varrho}_t(D)$ and where $p(D) = \mathrm{Tr}\{\hat{\varrho}_t(D)\}$ provides the probability distribution for outcome D to be measured.

Equation (35) is subdivisible into three main terms: the first term on the RHS represents the feedback controlled evolution, which takes the form of a Lindblad master equation and allows for arbitrary dependence on the measurement outcome D. The second term instead characterizes the decoherence of the system in the eigenbasis of observable $\hat{A}$. Lastly, the remaining two terms define a Fokker-Planck equation for the detector time evolution, where: the term proportional to γ represents the drift term with coefficient $\mathcal{A}(D)\hat{\varrho} \equiv \frac{1}{2}\left\{\hat{A} - D, \hat{\varrho}\right\}$, while the term proportional to γ^2 characterizes the diffusion of the probability distribution. The detector is therefore treated as a probability distribution in D-space. This distribution then drifts along D according to $-\gamma\mathcal{A}(D)\hat{\varrho}$, whilst its spread on D its dictated by the diffusion term $\frac{\gamma^2}{8\lambda}\partial_D^2\hat{\varrho}_t(D)$. In short, the detector is modelled as a stochastic walker relaxing towards a value dictated by the system state.

2.5.2 Separation of Time Scales

In general, Eq. (35) is typically limited to numerical integration. However, in this section we explore one additional approximation in order to recover an analytically treatable equation. This is achieved by separating the different time scales in Eq. (35). Each of the different terms in the RHS of Eq. (35) provides a different mechanism comprising the joint system plus detector dynamics. All of these mechanisms are then characterized by different time scales, that is: the measurement backaction is governed by a time scale $\vartheta_{\mathrm{ba}} \approx 1/\lambda$ while the detector evolution time scale scales as $\vartheta_{\mathrm{d}} \approx 1/\gamma$. Lastly, the feedback controlled evolution is governed by a time scale $\vartheta_{\mathrm{f}} \approx 1/\Lambda$, where Λ is the largest time scale defining parameter within $\mathcal{L}(D)\hat{\varrho}_t$. In the limit $\gamma \gg \Lambda, \lambda$, we then have $\vartheta_{\mathrm{d}} \ll \vartheta_{\mathrm{ba}}, \vartheta_{\mathrm{f}}$. This limit is understood as the instance in which the detector evolves much faster than the system, thus allowing for a complete resolution of the system dynamics. Note that if the chosen observable $\hat{A}$ introduces no backaction, we can safely neglect the $\gamma \gg \lambda$ limit. For $\gamma \gg \Lambda, \lambda$ we can, to leading order, write Eq. (35) as [54]

$$\partial_t\hat{\varrho}_t(D) \approx -\gamma\partial_D\mathcal{A}(D)\hat{\varrho}_t(D) + \frac{\gamma^2}{8\lambda}\partial_D^2\hat{\varrho}_t(D), \tag{36}$$

describing the dynamics of the detector. The stationary state of Eq. (36) can be written as

$$\hat{\varrho}_t(D) = \sum_{ij}\mathcal{G}_{ij}(D)\mathcal{V}_{ij}\hat{\varrho}_t, \tag{37}$$

where we introduced the projection operator $\mathcal{V}_{ij}\hat{\varrho} = \langle \mathrm{a}_i|\hat{\varrho}|\mathrm{a}_j\rangle|\mathrm{a}_i\rangle\langle\mathrm{a}_j| = \hat{\varrho}_{ij}|\mathrm{a}_i\rangle\langle\mathrm{a}_j|$ for the eigenstates of observable $\hat{A}$: $\hat{A}|\mathrm{a}_i\rangle = \mathrm{a}_i|\mathrm{a}_i\rangle$ and $\mathcal{G}_{ij}(D) = \sqrt{\frac{4\lambda}{\pi\gamma}}\exp(-\frac{4\lambda}{\gamma}(D - \frac{\mathrm{a}_i+\mathrm{a}_j}{2})^2)$. The stationary state of the detector $P(D) = \mathrm{Tr}\left\{\hat{\varrho}_t(D)\right\}$ is thus a combination of Gaussian curves centered at the eigenvalues of the observable. The interplay between λ and γ determines the noise of the detector. By replacing Eq. (37) into Eq. (35) and integrating over D leaves us

with a master equation for the evolution of the system alone

$$\partial_t \hat{\varrho}_t = \lambda \mathcal{D}[\hat{A}]\hat{\varrho}_t + \int_{-\infty}^{\infty} dD \mathcal{L}(D) \sum_{ij} \mathcal{G}_{ij}(D) \mathcal{V}_{ij} \hat{\varrho}_t. \tag{38}$$

In contrast to Eq. (35), by specifying the form for the feedback dependent term $\mathcal{L}(D)$, it is possible to solve the integral in the above differential equation.

3 Systems and Feedback Protocol

As stated, the motivation behind this thesis is to answer the question of whether the entanglement generation of the quantum thermal engines presented in Ref. [1] could be increased by the introduction of some continuous feedback protocol. To answer this question, we benchmark our results against results obtained in previous studies of the systems [1, 18]. The two engines considered in these are of two types: a bosonic thermal-bath-driven engine and a fermionic thermal-bath-driven engine. In this section, we therefore characterize these systems and discuss their dynamics in the absence of measurement and feedback. For each one of these we then include the levels of entanglement achievable under optimal choice of parameters for all discussed entanglement quantifiers. In this section we also present a detailed characterization of the studied protocol, highlighting its design and functionality.

3.1 The Bosonic Thermal Engine

The bosonic engine (Fig. 4) is comprised of two resonant qubits coherently coupled to each other with a strength denoted by g. The two qubits are separately coupled to two bosonic thermal reservoirs of temperature T_c and T_h, where $T_\mathrm{c} < T_\mathrm{h}$.

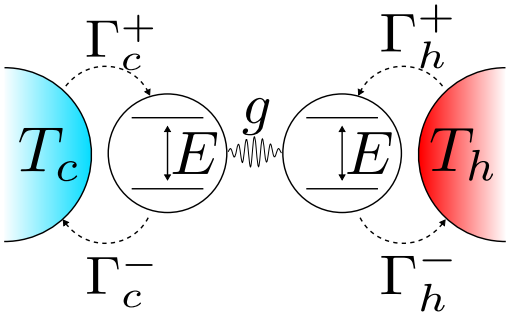

Figure 4: The bosonic thermal engine is comprised by two coherently interacting resonant qubit systems. In this engine two bosonic thermal reservoirs are separately coupled to the two qubits and a temperature bias is applied such that $T_\mathrm{h} > T_\mathrm{c}$.

To characterize the local states of the respective qubits we use the eigenbasis of the Pauli-z operator. With this choice of basis states, the system Hamiltonian takes the form

$$\hat{H} = E\left(|1\rangle\langle 1| \otimes \mathbb{1} + \mathbb{1} \otimes |1\rangle\langle 1|\right) + g\left(|01\rangle\langle 10| + |10\rangle\langle 01|\right), \tag{39}$$

where E is the energy spacing of either qubit (see Fig. 4) and will be set to $E = 1\ \mathrm{s}^{-1}$ in the rest of this thesis. The bipartite system evolves according to a Lindblad master equation (see Eq. (14)) of the form

$$\partial_t \hat{\varrho} = \mathcal{L}_\mathrm{B}\hat{\varrho}_t = -i\left[\hat{H}, \hat{\varrho}_t\right] + \sum_{\nu=\mathrm{c,h}} \left(\Gamma_\nu^+ \mathcal{D}[\hat{J}_\nu] + \Gamma_\nu^- \mathcal{D}[\hat{J}_\nu^\dagger]\right)\hat{\varrho}_t. \tag{40}$$

In the above, the Lindblad operators $\hat{J}_\nu$ ($\hat{J}_\nu^\dagger$) represent the processes by which the joint system can receive (lose) one excitation from the baths. More specifically, they take the form

$$\hat{J}_\mathrm{h} = \mathbb{1} \otimes \hat{\sigma}_+, \quad \hat{J}_\mathrm{c} = \hat{\sigma}_+ \otimes \mathbb{1}, \tag{41}$$

where $\hat{\sigma}_+ = |1\rangle\langle 0|$ and $\mathbb{1}$ is the identity operator. As an example, the Lindblad operator $\hat{J}_\mathrm{h}$ ($\hat{J}_\mathrm{h}^\dagger$) corresponds to the process through which the hot qubit absorbs (releases) one quantum of energy. The rates $\Gamma_\nu^\pm$ at which each of these processes occur, are then determined by the coupling strenghts Γ_c, Γ_h and the Bose-Einstein distribution of each environment

$$\Gamma_\mathrm{h}^+ = \Gamma_\mathrm{h} n_\mathrm{B}(T_\mathrm{h}), \tag{42}$$
$$\Gamma_\mathrm{c}^+ = \Gamma_\mathrm{c} n_\mathrm{B}(T_\mathrm{c}), \tag{43}$$
$$\Gamma_\mathrm{h}^- = \Gamma_\mathrm{h}(1 + n_\mathrm{B}(T_\mathrm{h})), \tag{44}$$
$$\Gamma_\mathrm{c}^- = \Gamma_\mathrm{c}(1 + n_\mathrm{B}(T_\mathrm{c})), \tag{45}$$

where $n_\mathrm{B}(T_\nu) = 1/(e^{E/T_\nu} - 1)$, T_ν is the temperature of bath ν and we have set $k_\mathrm{B} = 1$. Note that $\hat{\varrho}_t$ takes the form of Eq. (18). Most of the off-diagonals of $\hat{\varrho}_t$ can be put to zero as they are uncoupled from the rest of the elements, and thus vanish in the stationary limit because of bath induced dephasing. However, note that the system Hamiltonian (see Eq. (39)) coherently couples the subspace of the system spanned by the $|01\rangle$ and $|10\rangle$ states. This indicates that, in the long time limit, the system will have surviving coherences only within the coherently coupled subspace, as the coupling with the environments will degrade all other off-diagonal terms. More rigorously, we use Eq. (40) to write the dynamic equation for the coherences α within the coherently coupled subspace of the engine

$$\dot{\alpha} = ig(\hat{\varrho}_{01} - \hat{\varrho}_{10}) - \frac{1}{2}\left[\Gamma_\mathrm{c}\left(1 + 2n_\mathrm{B}(T_\mathrm{c})\right) + \Gamma_\mathrm{h}\left(1 + 2n_\mathrm{B}(T_\mathrm{h})\right)\right]\alpha, \tag{46}$$

where $\hat{\varrho}_{ij} \equiv \langle ij|\hat{\varrho}|ij\rangle$. Given a sufficiently high value of g, the coherent coupling is therefore capable of sustaining non-zero level of coherence within the coherently coupled subspace of the system. While, for stronger coupling to the baths, the dissipative term in Eq. (46) will take over, fully degrading also these coherences in the long time limit. In either case, the system will evolve to reach a steady state of the form of Eq. (18).

3.2 The Fermionic Thermal Engine

The fermionic engine is comprised of a double quantum dot, where the dots are coherently coupled to each other with a strength denoted by g. The dots have equal energy ε and are separately coupled to fermionic thermal reservoirs of temperature T_c and T_h, with $T_\mathrm{h} > T_\mathrm{c}$. Here, the energy levels of the dots are placed well above the chemical potential μ_ν of either bath. In this thesis we set $\mu_\mathrm{c} = \mu_\mathrm{h} = 0$ and $\varepsilon = 1$ s^{-1}. In order to describe the interaction between two fermions simultaneously inhabiting the two dots, a Coulomb repulsion proportional to U is added (see Fig. 5). We further assume a strong intra-dot Coulomb repulsion allowing only one fermion to occupy each dot at a time.

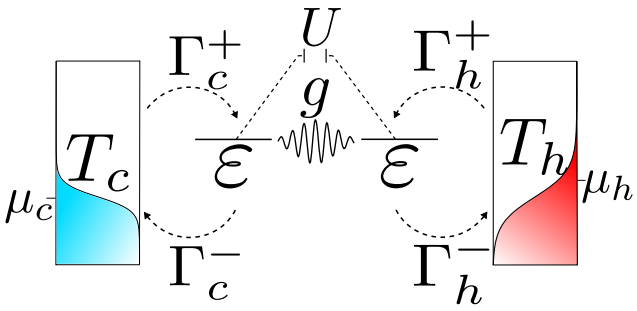

Figure 5: The fermionic thermal engine is comprised by two coherently coupled quantum dots. In this engine two fermionic thermal reservoirs are separately coupled to the two dots and a temperature bias is applied such that $T_\mathrm{h} > T_\mathrm{c}$.

To characterize the system, we use the basis $\{|0\rangle, |\mathrm{C}\rangle, |\mathrm{H}\rangle, |\mathrm{CH}\rangle\}$ respectively denoting the the states where no dot is occupied, only the cold dot is occupied, only the hot dot is occupied and both dots are simultaneously occupied. Using this basis, the system Hamiltonian takes the form

$$\hat{H} = \varepsilon\left(|\mathrm{C}\rangle\langle\mathrm{C}| + |\mathrm{H}\rangle\langle\mathrm{H}|\right) + g\left(|\mathrm{C}\rangle\langle\mathrm{H}| + |\mathrm{H}\rangle\langle\mathrm{C}|\right) + (2\varepsilon + U)\,|\mathrm{CH}\rangle\langle\mathrm{CH}|, \tag{47}$$

In Eq. (47), U represents the interdot Coulomb repulsion strength. This term has the effect of raising the energy cost for the doubly occupied state, thus limiting the population within this level.

The system dynamics are then dictated by a Lindblad master equation of the form

$$\mathcal{L}_\mathrm{F}\hat{\varrho}_t = -i\left[\hat{H}, \hat{\varrho}_t\right] + \sum_{\nu=\mathrm{c,h}}\left(\Gamma_\nu^+\mathcal{D}[\hat{J}_\nu] + \Gamma_\nu^-\mathcal{D}[\hat{J}_\nu^\dagger]\right)\hat{\varrho}_t + \mathcal{L}_\mathrm{CH}\hat{\varrho}_t. \tag{48}$$

In Eq. (48), the Lindblad operators $\hat{J}_\nu$ describe the processes through which fermions tunnel into either dot $\hat{J}_\mathrm{c} \equiv |\mathrm{C}\rangle\langle 0|$, $\hat{J}_\mathrm{h} \equiv |\mathrm{H}\rangle\langle 0|$. Note that the dissipator for these Lindblad operators act in a similar fashion to the ones in Eq. (40). In fact, it is possible to derive an analogous expression to Eq. (46) for the coherences within the coherently coupled subspace of the fermionic engine. From this, we would again see that for sufficiently strong coherent coupling g, the coherences within this subspace would survive, despite the coupling to the thermal baths. Thus, we conclude that, in the long time limit, this engine approaches the form of Eq. (18). The rates $\Gamma_\nu^\pm$ for the tunneling events are then characterized by the coupling strength to the respective bath Γ_ν and the Fermi-Dirac distribution $n_\mathrm{F}(T_\nu) = 1/(e^{(\varepsilon-\mu_\nu)/T_\nu}+1)$ for $\nu \in \{\mathrm{c,h}\}$

$$\Gamma_\nu^+ = \Gamma_\nu n_\mathrm{F}(T_\nu), \quad \Gamma_\nu^- = \Gamma_\nu(1 - n_\mathrm{F}(T_\nu)). \tag{49}$$

Lastly, the term $\mathcal{L}_\mathrm{CH}$ in Eq. (48) contains all information regarding the transitions involving the doubly occupied state $|\mathrm{CH}\rangle$. In appendix B, we provide the form for $\mathcal{L}_\mathrm{CH}$. From $\mathcal{L}_\mathrm{CH}$, we note that in the large U limit, the doubly occupied state takes on the profile of an exponential decaying function in time. In this thesis we focus on the scenario in which $U \to \infty$ thus, we can safely neglect the $\mathcal{L}_\mathrm{CH}$ term, as the doubly occupied state is prohibited.

3.3 Prior Work

In this section we report the results obtained in Refs. [1,18], for the steady state entanglement generation of the engines presented in Secs. 3.1 and 3.2. As discussed, the form taken by either engine in its steady state is given in Eq. (18). This implies that the concurrence of either engine is calculated through Eq. (19). The authors in Ref. [1] determine an optimal choice of parameters under which the steady state concurrence for the bosonic engine reaches $C(\hat{\varrho}_\infty) \approx 0.093$ (at $\Gamma_c^+ = 0$; $\Gamma_c^-/E = 0.01$; $\Gamma_h/E = 1.14 \cdot 10^{-4}$; $T_c/E = 0.01$), while, the steady state concurrence for its fermionic counterpart reaches $C(\hat{\varrho}_\infty) \approx 0.25$ (at $\Gamma_c^+ = 0$; $\Gamma_c^-/E = 0.05$; $\Gamma_h/E = 0.05$; $T_c/E = 0.01$; $U \to \infty$) (for a complete analytical treatment of the fermionic system's free evolution see appendix F). The heat maps shown in Fig. 6 portray the concurrence as a function of the inter-qubit strength g and the temperature of the hot bath T_h, for both the bosonic thermal engine (see Fig. 6.a) and its fermionic counterpart (see Fig. 6.b). We note that, in terms of concurrence, the fermionic engine outperforms its bosonic counterpart.

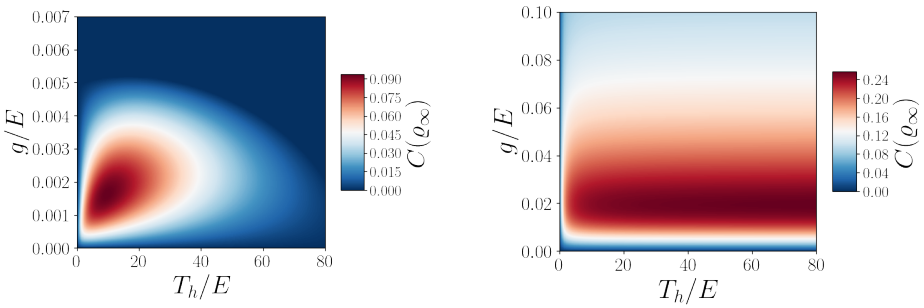

a) **b)**

Figure 6: Heat maps for the concurrence of the bosonic and fermionic thermal machines under choice of optimal parameters presented in Refs. [1]. Both maps were plotted as a function of the inter-qubit strength g and the temperature of the hot bath T_h. In their maximum region, the bosonic engine (**a)**) arrives at concurrence values up to $C(\hat{\varrho}_\infty) \approx 0.093$ (at $\Gamma_c^+ = 0$; $\Gamma_c^-/E = 0.01$; $\Gamma_h/E = 1.14 \cdot 10^{-4}$; $T_c/E = 0.01$), while its fermionic counterpart reaches $C(\hat{\varrho}_\infty) \approx 0.25$ (at $\Gamma_c^+ = 0$; $\Gamma_c^-/E = 0.05$; $\Gamma_h/E = 0.05$; $T_c/E = 0.01$; $U \to \infty$)

The difference in the concurrence generation of the two engines is to be attributed to the presence of interdot Coulomb repulsion within the fermionic system, which allows for more population to be transferred to the coherently coupled subspace (see Eq. (19)). Furthermore, the monotonic behaviour of the concurrence in the fermionic system as function of T_h is explained by studying the dephasing rates for the fermionic engine. From Eq. (48) we note that the coherences $\alpha \equiv \langle C|\hat{\varrho}|H\rangle$ within the coherently coupled subspace have the dynamical equation

$$\dot{\alpha} = ig\left(\hat{\varrho}_C - \hat{\varrho}_H\right) - \frac{1}{2}\left(\Gamma_c^- + \Gamma_h^-\right)\alpha \tag{50}$$

where $\hat{\varrho}_i \equiv \langle i|\hat{\varrho}|i\rangle$ for $i \in \{|C\rangle, |H\rangle\}$. From Eq. (50) we note that in the limit $T_h \to \infty$, the decay rate Γ_h^- approaches a constant value as it is proportional to the Fermi-Dirac distribution

$n_{\mathrm{F}}(T_{\mathrm{h}})$. On the other hand, the same is not true for the bosonic thermal engine. Equation (46) shows that for $T_{\mathrm{h}} \to \infty$ the dissipation within the system diverges as the Bose-Einstein distribution $n_{\mathrm{B}}(T_{\mathrm{h}})$ diverges with diverging temperature. This difference explains how the fermionic engine is capable of sustaining high concurrence values for higher temperatures, while the bosonic engine's concurrence degrades fairly quickly.

Although both engines do posses the ability of generating steady state entanglement, the authors of Ref. [18] demonstrate that the generated entanglement is not enough to neither perform teleportation with a high enough fidelity, nor portray non-local behaviours by violating the $CHSH$ inequality (see steady state obtained in Eq. (107)). In the next section we therefore introduce a feedback protocol capable of increasing the entanglement generation of both engines.

3.4 The Protocol

As illustrated in Fig. 7, the implemented feedback procedure is a two-step process. While Fig. 7 depicts the bosonic engine, an analogous illustration could be made using the fermionic engine. The protocol proceeds as follows: the system is allowed to freely evolve until the detector measures a single excitation within the two qubits ($D < 0$ in Fig. 7). When that happens, the hot bath is decoupled from the engine, thus preventing excitations from leaving to the hot bath. The coupling to the hot bath is then switched back on whenever the detector measures the bipartite qubit system in either the doubly ground state $|00\rangle\langle 00|$ or doubly excited state $|11\rangle\langle 11|$ ($D > 0$ in Fig. 7) .

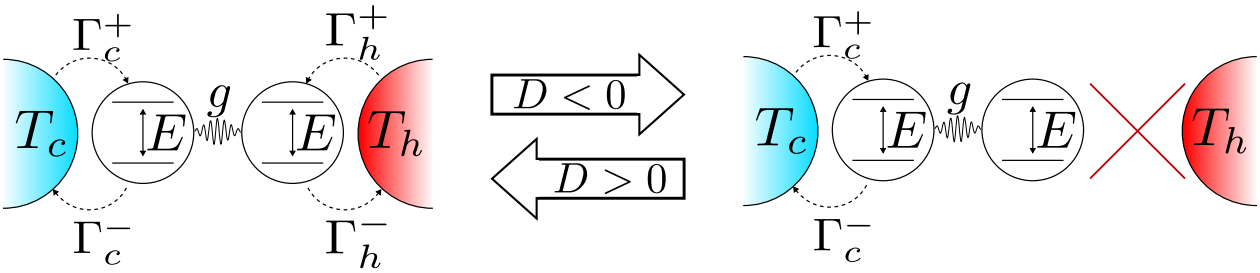

Figure 7: An illustration of the developped feedback protocol. This example is visualized for the bosonic engine. However, the reasoning holds for the fermionic engine as well. The system is left to evolve until a single excitation is measured within the bipartite qubit system (the observable used in the bosonic case is $\hat{A}_{\mathrm{B}} = |00\rangle\langle 00| + |11\rangle\langle 11| - (|01\rangle\langle 01| + |10\rangle\langle 10|)$). When that happens, the feedback forces the hot bath to decouple from the rest of the engine. If the qubit system is then detected in the doubly ground state $|00\rangle\langle 00|$ or doubly excited state $|11\rangle\langle 11|$, the feedback process recouples the hot bath to the rest of the open system.

The development of the protocol is the outcome of several intuitions. Firstly, as $T_{\mathrm{h}} > T_{\mathrm{c}}$ we expect most of the excitations to enter the system through the hot bath coupling. Therefore, by decoupling this bath, we force the majority of the excitations to be coherently exchanged between the two qubits (see Eq. (39)), thereby generating entanglement. Furthermore, by decoupling the hot bath, we decrease the bath induced decoherence.

To detect single excitations within the bosonic engine, we have selected the parity observable $\hat{A}_{\mathrm{B}} \equiv \hat{\sigma}_z \otimes \hat{\sigma}_z = |00\rangle\langle 00| + |11\rangle\langle 11| - (|01\rangle\langle 01| + |10\rangle\langle 10|)$, where $\hat{\sigma}_z$ is the Pauli-z operator. This observable returns outcomes $D > 0$ when the state is measured to have

more than one or no excitations, while it instead returns $D < 0$ when a single qubit lies in its excited state. Furthermore, continuous parity measurement on qubit systems have been demonstrated in laboratory settings, thus keeping this protocol experimentally relevant [55, 56]. For the fermionic engine, the observable used to detect single fermions then takes the form $\hat{A}_{\mathrm{F}} \equiv |0\rangle\langle 0| - (|\mathrm{C}\rangle\langle \mathrm{C}| + |\mathrm{H}\rangle\langle \mathrm{H}|)$. Although, seemingly arbitrary, one could think of this observable as corresponding to a charge detector symmetrically placed in between the dots to measure the presence of single fermions. As for the bosonic observable, the measure of $\hat{A}_{\mathrm{F}}$ returns outcomes $D > 0$ when the system is measured to contain no fermions, while it instead returns $D < 0$ when one fermion resides in the system. As for parity measurements, continuous charge detection measurements have also been realized in laboratory settings treating quantum dots systems [49].

The feedback procedure illustrated in Fig. 7 can be more rigorously formulated by setting the coupling strength Γ_{h} to be dependent on the filtered measurement outcome D through a Heaviside step function $\theta(D)$

$$\Gamma_{\mathrm{h}}(D) = \Gamma_{\mathrm{h}}\theta(D). \tag{51}$$

Through Eq. (51) we rewrite the term $\mathcal{L}(D)$ in Eq. (38) as

$$\mathcal{L}_q(D)\hat{\varrho} = \theta(D)\mathcal{L}_q(\Gamma_{\mathrm{h}})\hat{\varrho} + [1-\theta(D)]\mathcal{L}_q(\Gamma_{\mathrm{h}}=0)\hat{\varrho}, \tag{52}$$

where $q \in \{\mathrm{F}, \mathrm{B}\}$ labels which engine we are evolving. Inserting Eq. (52) into Eq. (38) allows us to perform the integration over all outcomes D

$$\partial_t\hat{\varrho}_t = \lambda\mathcal{D}[\hat{A}_q]\hat{\varrho}_t + \int_{-\infty}^{\infty} dD\mathcal{L}(D)\sum_{ij}\mathcal{G}_{ij}(D)\mathcal{V}_{ij}\hat{\varrho}_t \tag{53}$$

$$= \lambda\mathcal{D}[\hat{A}_q]\hat{\varrho}_t + \int_{-\infty}^{\infty} dD\left(\theta(D)\mathcal{L}_q + (1-\theta(D))\mathcal{L}_q(\Gamma_{\mathrm{h}}=0)\right)\sum_{ij}\mathcal{G}_{ij}(D)\mathcal{V}_{ij}\hat{\varrho}_t \tag{54}$$

$$= \lambda\mathcal{D}[\hat{A}_q]\hat{\varrho}_t + \left[\mathcal{L}_q\sum_{ij}\left(\int_0^{\infty} dD\mathcal{G}_{ij}(D)\right) + \mathcal{L}_q(\Gamma_{\mathrm{h}}=0)\sum_{ij}\left(\int_{-\infty}^{\infty} dD\mathcal{G}_{ij}(D)\right)\right.$$
$$\left. -\mathcal{L}_q(\Gamma_{\mathrm{h}}=0)\sum_{ij}\left(\int_0^{\infty} dD\mathcal{G}_{ij}(D)\right)\right]\mathcal{V}_{ij}\hat{\varrho}_t \tag{55}$$

$$= \lambda\mathcal{D}[\hat{A}_q]\hat{\varrho}_t + \mathcal{L}_\nu\mathcal{O}_q\hat{\varrho}_t + \mathcal{L}_q(\Gamma_{\mathrm{h}}=0)\hat{\varrho}_t - \mathcal{L}_q(\Gamma_{\mathrm{h}}=0)\mathcal{O}_q\hat{\varrho}_t. \tag{56}$$

In Eq. (56) we defined the superoperator $\mathcal{O}_q$ as being proportional to the feedback error probability $\eta \equiv \frac{1}{2}\left[1 - \mathrm{erf}\left(2\sqrt{\frac{\lambda}{\gamma}}\right)\right]$. Note that we interpret $\mathcal{O}_q$ as characterizing the error rates of the detector. That is, $\mathcal{O}_q$ describes the probability for the detector to erroneously apply feedback, given a measurement strength λ. Given the definition for η, we see that for high measurement strengths (i.e. $\lambda \gg \gamma$) $\eta \to 0$ and feedback is applied correctly. Instead, for low measurement strength values (i.e. $\lambda \ll \gamma$), $\eta \to \frac{1}{2}$. Here, little information can be extracted with each measurement, and feedback is randomly applied 50% of the times.

To describe the approach used to solve Eq. (56), we note that Eq. (56) is linear in the system representation $\hat{\varrho}_t$. Thus, the dynamics of the system can be rewritten in a vector

differential equation by vectorizing $\hat{\varrho}_t$ as ρ_t, so that

$$\partial_t \rho_t = \mathscr{L}_q \rho_t. \tag{57}$$

In Eq. (57), the Lindblad operator $\mathscr{L}_q$ is a $d \times d$ matrix, where d is the dimensionality of the vector ρ_t. From Eq. (56) it is straightforward to show that $\mathscr{L}_q$ preserves the Hermicity and normalization condition (7) of $\hat{\varrho}_t$. Additionally, rewriting Eq. (56) into a vector differential equation allows for a straightforward way to compute the steady state solution ρ_∞. By definition, $\partial_t \rho_\infty = 0$, and thus, the steady state solution corresponds to the eigenvector of the operator $\mathscr{L}_q$ with eigenvalue zero, or in other words, to the kernel of the matrix $\mathscr{L}_q$. In general, rewriting $\hat{\varrho}$ into a state vector ρ would lead us to deal with a 16-dimensional vector. However, upon few considerations, we can reduce the number of degrees of freedom that we need to study.

As mentioned, the steady state of either engine takes the form of Eq. (18). This suggests that, for steady state calculations, we can reduce our efforts to 6 degrees of freedom in the bosonic case, while, for the fermionic engine, we can reduce them to 5, as we consider the limit of $U \to \infty$, thereby prohibiting the $|\mathrm{CH}\rangle$ state. Thus, we unwrap the bosonic density operator $\hat{\varrho}$ as $\rho = (\hat{\varrho}_{00}, \hat{\varrho}_{01}, \hat{\varrho}_{10}, \hat{\varrho}_{11}, \alpha, \alpha^*)^T$, where $\hat{\varrho}_{ij} \equiv \langle ij|\hat{\varrho}|ij\rangle$ and $\alpha \equiv \langle 10|\hat{\varrho}|10\rangle$. Under this unwrapping, the error superoperator $\mathcal{O}_\mathrm{B}$ takes on the form of a diagonal matrix $\mathcal{O}_\mathrm{B} \equiv \mathrm{diag}(1-\eta, \eta, \eta, 1-\eta, \eta, \eta)$, while the Lindblad superoperator $\mathscr{L}_\mathrm{B}$ takes the form

$$\mathscr{L}_\mathrm{B} = \begin{bmatrix} -\Gamma_\mathrm{c}^+ - (1-\eta)\Gamma_\mathrm{h}^+ & \eta\Gamma_\mathrm{h}^- & \Gamma_\mathrm{c}^- & 0 & 0 & 0 \\ (1-\eta)\Gamma_\mathrm{h}^+ & -\eta\Gamma_\mathrm{h}^- - \Gamma_\mathrm{c}^+ & 0 & \Gamma_\mathrm{c}^- & ig & -ig \\ \Gamma_\mathrm{c}^+ & 0 & -\Gamma_\mathrm{c}^- - \eta\Gamma_\mathrm{h}^+ & (1-\eta)\Gamma_\mathrm{h}^- & -ig & ig \\ 0 & \Gamma_\mathrm{c}^+ & \eta\Gamma_\mathrm{h}^+ & -(1-\eta)\Gamma_\mathrm{h}^- - \Gamma_\mathrm{c}^- & 0 & 0 \\ 0 & ig & -ig & 0 & -\frac{1}{2}\left(\Gamma_\mathrm{c}^+ + \Gamma_\mathrm{c}^- + \eta\Gamma_\mathrm{h}^+ + \eta\Gamma_\mathrm{h}^-\right) & 0 \\ 0 & -ig & ig & 0 & 0 & -\frac{1}{2}\left(\Gamma_\mathrm{c}^+ + \Gamma_\mathrm{c}^- + \eta\Gamma_\mathrm{h}^+ + \eta\Gamma_\mathrm{h}^-\right) \end{bmatrix}. \tag{58}$$

For the fermionic engine, we unwrap the matrix representation of $\hat{\varrho}$ as a one-dimesional vector $\rho = (\hat{\varrho}_0, \hat{\varrho}_\mathrm{C}, \hat{\varrho}_\mathrm{H}, \alpha, \alpha^*)$, where $\hat{\varrho}_j \equiv \langle j|\hat{\varrho}|j\rangle$ for $j \in \{0, \mathrm{C}, \mathrm{H}\}$ and $\alpha \equiv \langle \mathrm{C}|\hat{\varrho}|\mathrm{H}\rangle$. With this unrapping, the error superoperator takes the form $\mathcal{O}_\mathrm{F} = \mathrm{diag}(1-\eta, \eta, \eta, \eta, \eta)$, whilst Eq. (56) can be reformulated as a vector differential equation $\partial_t \rho_t = \mathscr{L}_\mathrm{F} \rho_t$, where

$$\mathscr{L}_\mathrm{F} = \begin{bmatrix} -(1-\eta)\Gamma_\mathrm{h}^+ - \Gamma_\mathrm{c}^+ & \Gamma_\mathrm{c}^- & \eta\Gamma_\mathrm{h}^- & 0 & 0 \\ \Gamma_\mathrm{c}^+ & -\Gamma_\mathrm{c}^- & 0 & ig & -ig \\ (1-\eta)\Gamma_\mathrm{h}^+ & 0 & -\eta\Gamma_\mathrm{h}^- & -ig & ig \\ 0 & ig & -ig & -\frac{1}{2}\left(\Gamma_\mathrm{c}^- + \eta\Gamma_\mathrm{h}^-\right) & 0 \\ 0 & -ig & ig & 0 & -\frac{1}{2}\left(\Gamma_\mathrm{c}^- + \eta\Gamma_\mathrm{h}^-\right) \end{bmatrix}. \tag{59}$$

In both Eqs. (58), (59) we note the absence of an explicit dependence on λ (i.e. without accounting for η). This is explained by the choice of observables $\hat{A}_q$. In both cases, the chosen observable does not provide any backaction in the coherently coupled subspaces of the system, (i.e. $\mathcal{D}[\hat{A}_q] = 0$). This feature is qualitatively explained by the impossibility of using $\hat{A}_q$ to distinguish within which qubit (dot) are the excitations (fermions) lying.

4 Results

In this section, we present the results obtained for the systems discussed in chapter 3. Firstly, we present analytical results for the steady state of each system. Then, we analyze how robust the results are under different non-ideal conditions. We specifically consider imperfect isolation, where the hot bath is only partially isolated from the hot qubit. We also investigate the effect of an additional external environment on the obtained results. Finally, we study the behavior of the systems in the transient regime. This enables us to determine whether any of the steady states can be achieved in a finite amount of time.

4.1 Fermionic System

Here we present the results obtained for the feedback controlled evolution of the fermionic system presented in Sec. 3.2. The null-space of the Lindbladian expressed in Eq. (59) takes the form of Eq. (18), where

$$\varrho_0 = \left(\Gamma_{\mathrm{c}}^- + \Gamma_{\mathrm{h}}^- \eta\right)\left(\Gamma_{\mathrm{c}}^- \Gamma_{\mathrm{h}}^- \eta + 4g^2\right), \tag{60}$$

$$\varrho_1 = \left(\Gamma_{\mathrm{c}}^+ \Gamma_{\mathrm{h}}^- \eta\left(\Gamma_{\mathrm{c}}^- + \Gamma_{\mathrm{h}}^- \eta\right) + 4g^2\left(\Gamma_{\mathrm{c}}^+ + \Gamma_{\mathrm{h}}^+ (1-\eta)\right)\right), \tag{61}$$

$$\varrho_2 = \left(\left(\Gamma_{\mathrm{c}}^-\right)^2 \Gamma_{\mathrm{h}}^+ (1-\eta) + \Gamma_{\mathrm{c}}^- \Gamma_{\mathrm{h}}^+ \Gamma_{\mathrm{h}}^- \eta\,(1-\eta) + 4g^2\left(\Gamma_{\mathrm{c}}^+ - \Gamma_{\mathrm{h}}^+ (1-\eta)\right)\right), \tag{62}$$

$$\varrho_3 = 0, \tag{63}$$

$$\alpha = -2ig\left(\Gamma_{\mathrm{c}}^- \Gamma_{\mathrm{h}}^+ (1-\eta) - \Gamma_{\mathrm{c}}^+ \Gamma_{\mathrm{h}}^- \eta\right), \tag{64}$$

where the normalization constant is $\mathcal{N} = \varrho_0 + \varrho_1 + \varrho_2$. Using Eq. (19) to obtain the steady state concurrence for this system, leads us to the expression $C(\hat{\varrho}_\infty) = 2|\alpha|\mathcal{N}$. Thus, through Eq. (64) we note that, for this system, the concurrence is a monotonically increasing function of the measurement strength λ. This arises as consequence of choosing the operator $\hat{A}_{\mathrm{F}}$ as the measured observable. In Sec. 3.4, we discussed how the backaction from measuring this observable is null within the coherently coupled subspace. This property is reflected by the monotonic increasing nature of $C(\hat{\varrho}_\infty)$ with respect to λ. This suggests us to consider the limit $\lambda \to \infty$, thus recovering projective measurements for this choice of observable (see Sec. 2.4). Within the projective limit the detector is capable of correctly capturing the state of the system with null uncertainty in the measurement outcome, thus leading to correctly applied feedback at all times. Lastly, in order to obtain optimal entanglement generation we set $T_{\mathrm{c}} \to 0$ [1, 18]. Here the concurrence is expressed as

$$C(\hat{\varrho}_\infty) = 2|\alpha|\mathcal{N} \tag{65}$$

$$= \frac{g\Gamma_{\mathrm{c}}\Gamma_{\mathrm{h}}^+}{g^2\left(\Gamma_{\mathrm{c}} + 2\Gamma_{\mathrm{h}}^+\right) + \frac{1}{4}\Gamma_{\mathrm{c}}^2\Gamma_{\mathrm{h}}^+}. \tag{66}$$

An analytical derivation of the maximal concurrence is found by solving the system of equations established by $\nabla C(\hat{\varrho}_\infty) = 0$, where $\nabla \equiv (\partial_g, \partial_{\Gamma_{\mathrm{c}}}, \partial_{\Gamma_{\mathrm{h}}^+})$. By doing so, we note that $C(\hat{\varrho}_\infty)$ is a monotonically increasing function of Γ_{h}^+. As the Fermi-Dirac distribution is bounded, $C(\hat{\varrho}_\infty)$ is maximized in $\Gamma_{\mathrm{h}} \to \infty$. Thereby, the results shown in this section are derived in the limit $\Gamma_{\mathrm{h}} \gg \Gamma_{\mathrm{c}}$. However, in later sections we relax this assumption.

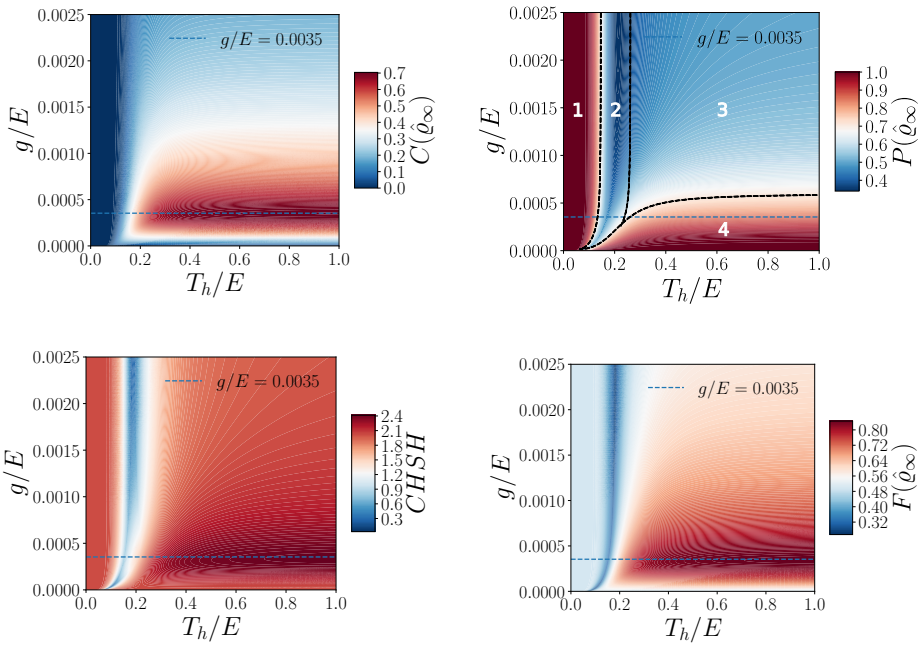

Figure 8: Heat maps obtained of the analytical results for the fermionic system. The maps show the steady state concurrence, purity, CHSH inequality or singlet fraction change as a function of the interdot interaction strength g and the temperature of the hot bath T_h. As per the analytical derivations, the concurrence graph shows the maximum concurrence to lie at around $C(\hat{\varrho}_\infty) = \frac{1}{\sqrt{2}}$. Whithin the same region, the CHSH inequality reaches valeus CHSH ≈ 2.4, while the singlet fraction reaches $F \approx 0.85$. The dashed line in each plot represents the value of g for optimal concurrence. In addition, each plot can be subdivided into four separate regions, as highlighted in the purity plot. Here we use $\Gamma_\mathrm{c}^-/E = 10^{-3}$; $\Gamma_\mathrm{h} = 100\Gamma_\mathrm{c}$; $T_c/E = 10^{-2}$.

In Fig. 8, we plot the concurrence, purity, CHSH value and singlet fraction for the fermionic system as function of the coherent coupling strength g and temperature of the hot bath T_h. Let us firstly focus on the results obtained for the concurrence. Here, we note the monotonically increasing behaviour of $C(\hat{\varrho}_\infty)$ with respect to T_h for any fixed g. This result is in agreement with the observation made for the behaviour of $C(\hat{\varrho}_\infty)$ with respect to Γ_h^+. Additionally, we also note the presence of a high concurrence region; within the considered limits, we derived an analytical expression for $C(\hat{\varrho}_\infty)$ enclosed by this area

$$C(\hat{\varrho}_\infty) = \frac{4g\Gamma_\mathrm{c}}{8g^2 + \Gamma_\mathrm{c}^2}. \tag{67}$$

We now observe that the maximum solution is found to be at $g = \frac{\Gamma_\mathrm{c}}{2\sqrt{2}}$ (see dashed line in Fig. 8). This solution for g corresponds to the high concurrence region of Fig. 8, where we obtain an analytical value of $C(\hat{\varrho}_\infty) = \frac{1}{\sqrt{2}}$. Within the same region, we see that the CHSH value reaches values around ~ 2.43 while the singlet fraction approaches ~ 0.85. In both cases, the obtained values lie well above the lower bounds set in Sec. 2.2, and the stationary state can be considered as non-classical.

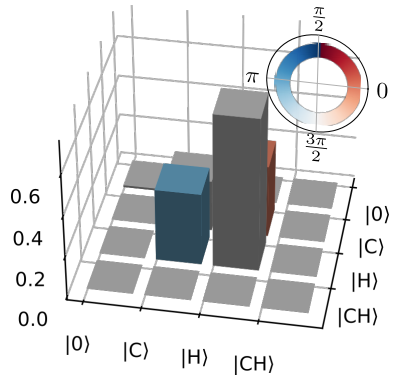

Figure 9: The system's steady state in the region of high concurrence (see region 4 within purity plot of Fig. 8). In this region the state populations are nearly completely reshuffled within the coupled subspace of the system, thus approaching the form of a pure Bell state (see Fig. 1.a).

Through the purity plot displayed in Fig. 8, we note that within the same region of optimal concurrence, the purity increases due to the feedback protocol. Figure 9 is a stationary state within the high concurrence region of Fig. 8. We see that the state is similar to the form of the maximally entangled Bell state $|\Psi_{\pm}\rangle$ in Eq. (15). Furthermore, from Fig. 9, we see that the strong interdot Coulomb repulsion is prohibiting the doubly occupied state $|\mathrm{CH}\rangle$, thus allowing for more population to be reshuffled within the desired subspace.

All of the heat maps in Fig. 8 share a similar contour profile, which allows us to equally divide each of them into four separate regions, as illustrated in the purity plot of Fig. 8. In Fig. 10 we show four bar plots for $\hat{\varrho}_{\infty}$ corresponding to each region.

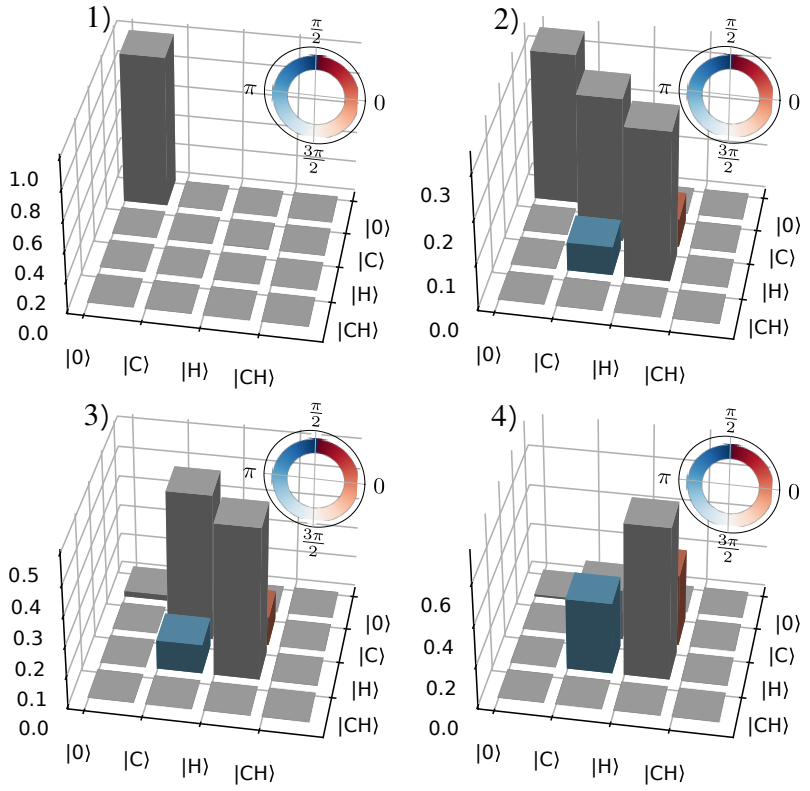

Figure 10: Four example system state representations for the four highlighted regions in the purity plot of Fig. 8.

To establish the origin of the highlighted regions, we note that each of these is characterized by a separate parameter regime. For instance, let us consider the region labelled by the index "1". As $T_{\rm h} \to 0$, we reach unit purity since since $\Gamma_{\rm h}^{+} \to 0$, which reduces the possibility of occupying the hot qubit, as no fermion can enter the system. The system thus resides in the pure state $|0\rangle\langle 0|$. The second highlighted region is characterized by low purity, indicating a highly mixed state. The state representation confirms this by showing that all allowed levels share an equivalent amount of population (see Fig. 10). Here, the hot bath temperature sets an equivalence between the jump-in and jump-out rates $\Gamma_{\rm h}^{+} \approx \Gamma_{\rm c}^{-}$. Therefore, $\hat{\varrho}_0 = \hat{\varrho}_1 \approx \hat{\varrho}_2$ as can be see from Eqs. (60)-(62). Region 3 is denoted by low purity and concurrence. In this region, $g \geq \Gamma_{\rm h}^{+}, \Gamma_{\rm h}^{-}$, favoring Rabi oscillations between the cold and hot qubit. For fast oscillations, the coherence is suppressed by phase averaging, as discussed in [57], thereby leading to low concurrence. The fourth region is the high entanglement region. In this region, the balance between incoherent and coherent interactions allows for a buildup of coherence, thus leading to higher concurrence.

4.2 Bosonic System

Here we present the results for the bosonic thermal machine presented in Sec. 3.1. The null-space of the Lindbladian shown in Eq. (58) is derived to be in the form of Eq. (18). As the measurement produces no backaction, we again consider an infinite measurement strength

$\lambda \to \infty$, such that feedback is applied correctly at all times. By again considering the limit $T_c \to 0$ we find the system steady state to be

$$\hat{\varrho}_\infty = \mathcal{N} \begin{bmatrix} g^2\Gamma_c & 0 & 0 & 0 \\ 0 & \left(\frac{1}{4}\Gamma_c^2 + g^2\right)\Gamma_h^+ & \frac{i}{2}g\Gamma_c\Gamma_h^+ & 0 \\ 0 & -\frac{i}{2}g\Gamma_c\Gamma_h^+ & g^2\Gamma_h^+ & 0 \\ 0 & 0 & 0 & 0 \end{bmatrix}, \tag{68}$$

where $\mathcal{N} = \left[\Gamma_c g^2 + \left(2g^2 + \frac{1}{4}\Gamma_c^2\right)\Gamma_h^+\right]^{-1}$ is a normalization factor. The concurrence of Eq. (68) reads

$$C(\hat{\varrho}_\infty) = \frac{g\Gamma_c\Gamma_h^+}{g^2\left(\Gamma_c + 2\Gamma_h^+\right) + \frac{1}{4}\Gamma_c^2\Gamma_h^+}. \tag{69}$$

This equation coincides with Eq. (66). In fact, as we will see, many of the results for the fermionic and bosonic engines are equivalent when $\lambda \to \infty$. To find the maximum concurrence, we solve the system of equations $\nabla C(\hat{\varrho}_\infty) = 0$, and find again, as for the fermionic engine, that $C(\hat{\varrho}_\infty)$ is a monotonically increasing function, that approaches its maximum as $\Gamma_h^+ \to \infty$. In Fig. 11, we plot the concurrence, purity, CHSH value and singlet fraction under the condition of $\Gamma_h \gg \Gamma_c$ as function of g and T_h.

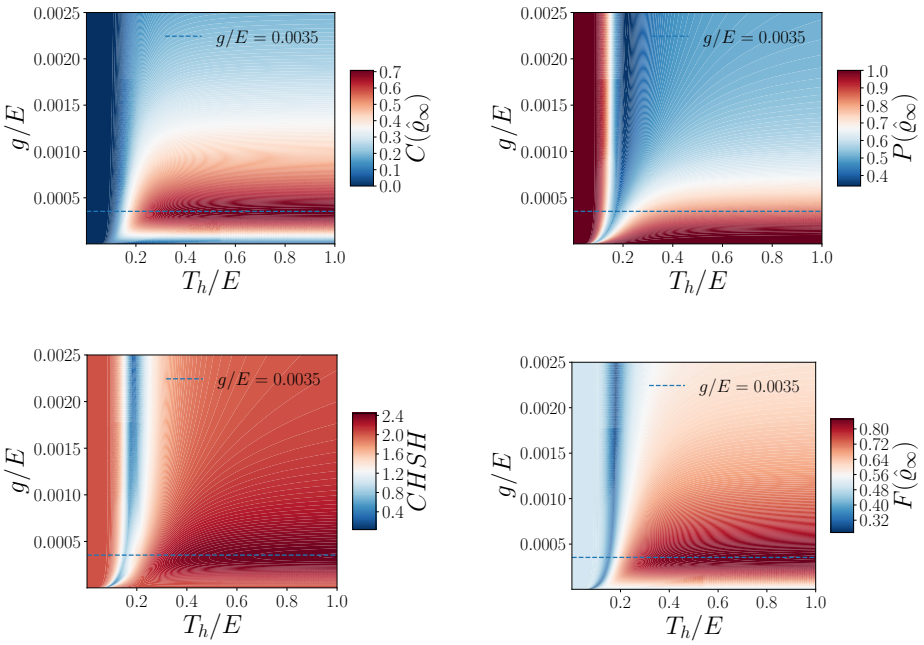

Figure 11: Heat maps of the analytical results, for the bosonic system. The maps show how the steady state concurrence, purity, CHSH inequality or singlet fraction change as a function of the interdot interaction strength g and the temperature of the hot bath T_h. As per the analytical derivations, the optimal values across all entanglement measures exactly match with those obtained in Fig. 8. The dashed line in each plot represents the value of g for optimal concurrence. Here we use $\Gamma_c^-/E = 10^{-3}$; $\Gamma_h = 100\Gamma_c$; $T_c/E = 10^{-2}$.

As for the results obtained for the fermionic thermal machine, we note that the concurrence presents a high concurrence region, for which we derived the analytical expression in the limit

$\Gamma_h \gg \Gamma_c$

$$C(\hat{\varrho}_\infty) = \frac{4g\Gamma_c}{8g^2 + \Gamma_c^2}. \tag{70}$$

Equation (70) has its maximum, at $g = \frac{\Gamma_c}{2\sqrt{2}}$ (see dashed line in Fig. 11), where $C(\hat{\varrho}_\infty) = \frac{1}{\sqrt{2}}$. By studying the singlet fraction and CHSH we find that these quantities have the same value as in the fermionic engine (i.e. CHSH ≈ 2.43 and $F \approx 0.85$). Lastly, from Fig. 11, we note that, within the region of high entanglement, the stationary state (depicted in Fig. 12) is similar to the maximally entangled Bell state $|\Psi_\pm\rangle$ of Eq. (15).

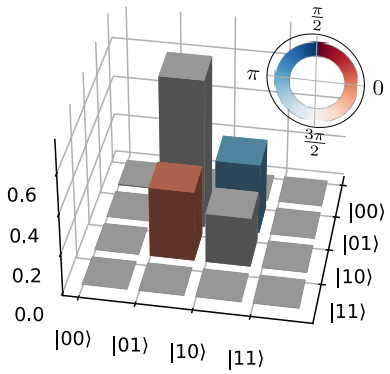

Figure 12: The system's steady state in the region of high concurrence (see concurrence plot in Fig. 11). In this region the state populations are nearly completely reshuffled within the coupled subspace of the system, thus approaching a maximally entangled Bell state (see Fig. 1.a).

By comparing the results of Secs. 4.1 and 4.2, we see that the two engines perform equivalently. This is in contrast to Sec. 3.3, where the fermionic engine produced a higher concurrence in the absence of measurement and feedback. The equivalence is a result of the assumptions $T_c \to 0$, $\lambda \to \infty$ and $\gamma \gg \max\{g, \Gamma_c, \Gamma_h\}$. In this regime, the stationary states of both engines are prohibited from occupying the doubly excited state, even when the Coulomb repulsion is set to $U = 0$ in the fermionic case. To understand why this is the case, we study the Liouvillian for the Bosonic engine in the limits $T_c \to 0$, $\lambda \to \infty$ and $\gamma \gg \max\{g, \Gamma_c, \Gamma_h\}$

$$\mathscr{L}_B = \begin{bmatrix} -\Gamma_h^+ & 0 & \Gamma_c^- & 0 & 0 & 0 \\ \Gamma_h^+ & 0 & 0 & \Gamma_c^- & ig & -ig \\ 0 & 0 & -\Gamma_c^- & \Gamma_h^- & -ig & ig \\ 0 & 0 & 0 & -\Gamma_c^- - \Gamma_h^- & 0 & 0 \\ 0 & ig & -ig & 0 & -\frac{1}{2}\Gamma_c^- & 0 \\ 0 & -ig & ig & 0 & 0 & -\frac{1}{2}\Gamma_c^- \end{bmatrix}. \tag{71}$$

From Eq. (71) we see that under the listed assumptions, the equation of motion for state $|11\rangle\langle 11|$ takes the profile of an exponential decay

$$\hat{\varrho}_{11}(t) \propto e^{-\left(\Gamma_h^- + \Gamma_c^-\right)t}, \tag{72}$$

thus explaining the lack of $|11\rangle\langle 11|$ population in the system steady state. This quantitative explanation suggests that the protocol is capable of recovering the behavior of a Coulomb

interaction-like term for the bosonic system, without requiring us to manually introduce it into the equations.

In order to obtain a more qualitative understanding of why the $|11\rangle\langle 11|$ state is prohibited, we have schematized an illustration in Fig. 13 representing the transitions described by the Liouville superoperator in Eq. (71).

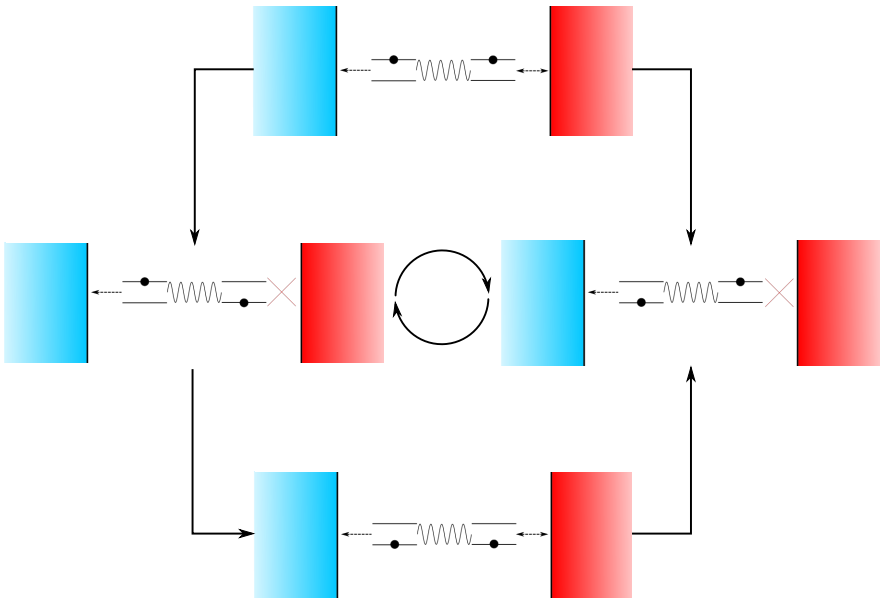

Figure 13: A schematic illustration of the transition described by the Liouville superoperator in Eq. (71). From this illustration we see that the doubly excited state is achievable as an initial condition for the machine, although the evolution does not allow transitions through this state.

Let us consider the system initialized in the doubly excited state (see Fig. 13). As per our assumptions, the detector has the ability to promptly and accurately distinguish this state. Here, the feedback protocol does not activate as $\theta(D > 0) = 1$. The system dynamics remain unchanged until one of the qubit loses its excitation to the respective bath, at which point $\theta(D < 0) = 0$, thereby terminating the connection with the hot bath. As the temperature of the cold bath is assumed to be zero, the excitation rate from the cold bath into the system is zero (i.e. $\Gamma_c^+ = 0$). As a result of the hot bath's complete decoupling from the system, any remaining excitation can only exit the system through the coupling with the cold bath. When this occurs, the detector responds immediately and accurately to the change by reconnecting the hot bath to the system ($\theta(D > 0) = 1$). The system then continues to evolve through chains of states that will never include the $|11\rangle\langle 11|$ state.

It is important to emphasize that the appearance of this effect is highly dependent on the simultaneous realization of all three assumptions concerning λ, γ, and T_c. If T_c were set to any value other than zero, the cold bath would be able to supply excitations to the system, leading to transitions $|01\rangle\langle 01| \to |11\rangle\langle 11|$. Additionally, if λ were set to a finite value, the detector might fail to detect excitations within the system, leaving the coupling to the hot bath open. Lastly, if γ was not set to be the largest parameter, a slower detector response time would allow for an excitation to be redistributed within the system before the coupling to the hot bath was shut.

4.3 A Different Parameter Regime

The results obtained in Sec. 4.1 and 4.2 reveal a symmetry between the entanglement generation of the two engines. This attribute has us wondering whether the feedback protocol makes the two engines equivalent. To address this question we explore a different parameter regime than the one studied in Sec. 4.1 and 4.2, by adjusting the values of Γ_c and Γ_h, whilst keeping the remaining parameters fixed. In Fig. 14, we illustrate the steady state concurrence for both the bosonic (Fig. 14.a) as well as the fermionic (Fig. 14.b) thermal machines as a function of the hot bath temperature, for different choices of coherent coupling strength g.

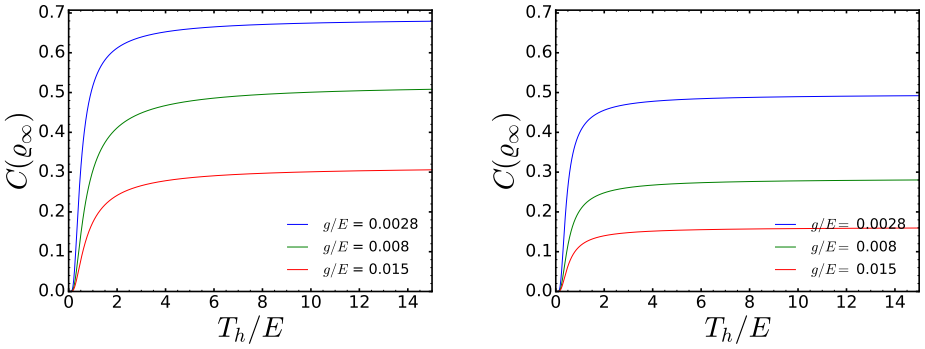

Figure 14: Graphs illustrating the concurrence as a function of T_h for both the bosonic thermal machine (**a**)) and the fermionic thermal machine (**b**)). The graphs were obtained in the parameter regime $\Gamma_h = \Gamma_c$. Here, the bosonic thermal mahcine produces higher concurrence than its fermionic counterpart in terms of entanglement generation. Here we used $\Gamma_c^+ = 0$; $\Gamma_c^-/E = 10^{-2}$; $\Gamma_h = \Gamma_c$; $T_c/E = 10^{-2}$; $\lambda \to \infty$.

To obtain the results shown in Fig. 14 we relax the requirement of $\Gamma_h \gg \Gamma_c$ by setting $\Gamma_h = \Gamma_c$, whilst keeping $\lambda \to \infty$. As a result, we see that, the bosonic thermal engine outperforms its fermionic analog, which disproves the notion of the two machines performing equivalently under the feedback protocol.

To explain the origin of this discrepancy, we derived an analytical expression that establishes a relation between the thermal heat current from the hot bath and the concurrence of each respective machine (refer to appendix G for a derivation)

$$C_F(\hat{\varrho}_\infty) = \frac{\dot{Q}_h}{g\varepsilon}, \qquad C_B(\hat{\varrho}_\infty) = \frac{\dot{Q}_h}{gE}. \tag{73}$$

The derived expression provides a useful insight for the relation between heat current and concurrence. The concurrence can be directly inferred by measuring the heat current and does not require quantum state tomography. Equation (73) further explains why the bosonic engine outperforms the fermionic one in Fig. 14. As $T_h \to \infty$

$$\Gamma_h^+ \to \begin{cases} \Gamma_h/2 & \text{Fermions} \\ \infty & \text{Bosons} \end{cases} \tag{74}$$

and the heat current is allowed to reach higher values in the bosonic engine than in the fermionic one, thereby explaining why the bosonic system can generate more entanglement.

It has to be noted that Eq. (73) remains valid also when relaxing the condition $\lambda \to \infty$ for the fermionic engine. This is because the high interdot Coulomb repulsion prohibits the doubly excited state.

4.4 Imperfect Isolation

Here we study the effect of imperfect isolation of the hot bath. Specifically, we examine the entanglement generation when the hot bath is partially isolated. To achieve this, we propose a variation of the protocol in which

$$\Gamma_{\rm h}(D) = \Gamma_{\rm h}\theta(D) + (\Gamma_{\rm h} - \delta)\,[1 - \theta(D)] \tag{75}$$

where $0 \leq \delta \leq \Gamma_{\rm h}$ is a constant, representing the degree of imperfect isolation. This analysis is of experimental relevance, where perfect isolation can be hard to achieve.

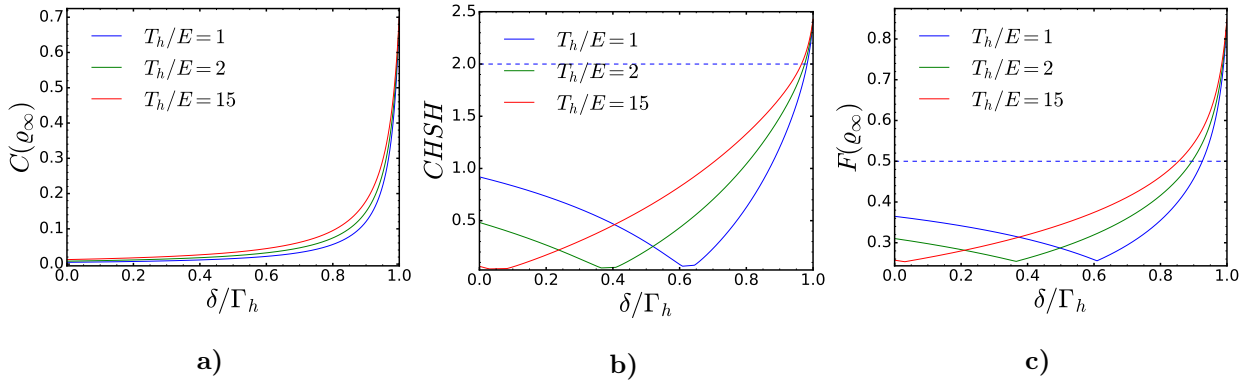

Figure 15: These plots show the concurrence, CHSH value and singlet fraction of the fermionic thermal machine as function of δ, for different choices of temperature of the hot bath $T_{\rm h}$. Here we see the effect of only partly isolating the hot bath from the system. Here we used $\Gamma_{\rm c}^{-}/E = 10^{-3}$; $\Gamma_{\rm h} = 100\Gamma_{\rm c}$; $T_c/E = 10^{-2}$; $g/E = 3.5 \cdot 10^{-4}$

Figure 15 portrays the concurrence (Fig. 15.a), CHSH value (Fig. 15.b), and singlet fraction (Fig. 15.c) of the fermionic thermal machine as a function of δ, at varying temperatures of the hot bath $T_{\rm h}$. The dashed lines in Figs. 15.b, 15.c highlight the lower bounds for classical behaviour. From Fig. 15, we can deduce that higher values of $T_{\rm h}$ result in a more favorable level of entanglement within the system, aligning with the findings in Sec. 4.1. It is noteworthy that regardless of the chosen temperature, Fig. 15 illustrates that the isolation level required for the system state to possess a useful quantity of entanglement must be above 80%. This highlights the significance of appropriate isolation in the optimization of entanglement generation in the fermionic thermal machine.

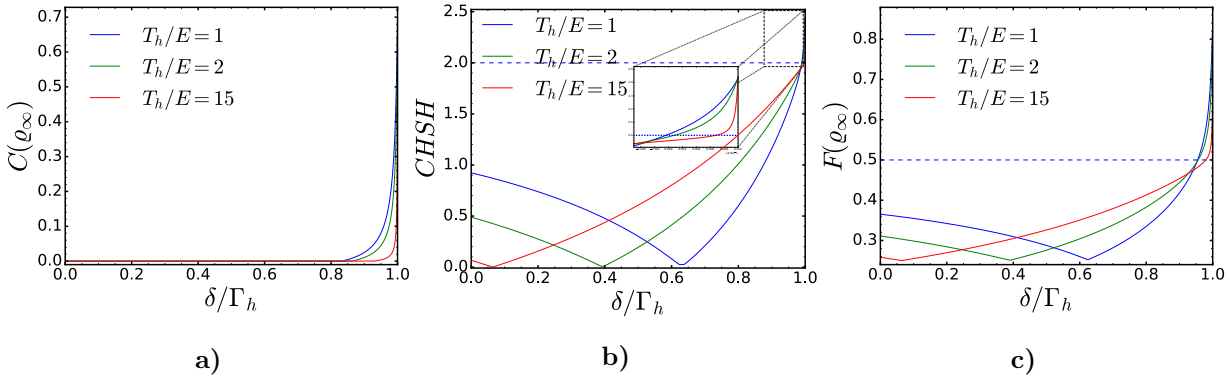

Figure 16: These plots show the concurrence, CHSH value and singlet fraction of the bosonic thermal machine as function of δ, for different choices of temperature of the hot bath T_h. Here we see the effect of only partly isolating the hot bath from the system. Here we used $\Gamma_\mathrm{c}^-/E = 10^{-3}$; $\Gamma_\mathrm{h} = 100\Gamma_\mathrm{c}$; $T_c/E = 10^{-2}$; $g/E = 3.5 \cdot 10^{-4}$

Figure 16 illustrate the concurrence (Fig. 16.a), CHSH value (Fig. 16.b) and singlet fraction (Fig. 16.c) of the bosonic thermal machine as function of δ, for various hot bath temperatures T_h. In contrast to the fermionic engine, there are significant differences. Firstly, the fermionic machine achieves non-zero concurrence at considerably lower isolation values, than the bosonic machine. Additionally, we note that the system must be above 95% isolated to contain any useful amount of entanglement. Lastly, unlike the fermionic machine, for the bosonic machine, different T_h values have varying impacts on different entanglement measures. This scenario is analogous to the free evolution case, where the bosonic thermal machine had an optimal hot bath temperature (see Sec. 3.3), as the dephasing within the bosonic machine becomes dependent on T_h.

In the context of imperfect conditions, an interesting difference between the bosonic and fermionic thermal machines arises. Specifically, in the imperfect isolation regime, the bosonic engine can become doubly excited, as the hot bath can provide excitations even when another excitation is already present. This is not the case for the fermionic machine, where the infinite Coulomb repulsion term prohibits the doubly excited state, thus allowing for a higher level of entanglement. This disparity is evident in the graphs presented in this section, where the absence of the Coulomb repulsion term in the bosonic machine reduces the amount of entanglement it can produce at lower isolation proportions. Thereby, under these conditions, the fermionic machine is again capable of outperforming its bosonic counterpart in terms of entanglement production.

4.5 Robustness Against External Decoherence

In this section, we present a model to investigate the impact of external dephasing. This was approached within the same parameter regime explored in Sec. 4.1 and 4.2. To model external decoherence, we introduce an exponential dampening term for the coherences (see Eqs. (58),(59)) via the inclusion of an additional damping term Γ_φ, such that

$$\dot{\alpha} = ig(\hat{\varrho}_{01} - \hat{\varrho}_{10}) - \frac{1}{2}\left(\Gamma_\mathrm{c}^- + \Gamma_\varphi\right)\alpha. \tag{76}$$

Although, this treatment of the exponential dampening term might appear arbitrary, it is important to note that a microscopical derivation for this model was provided in Ref. [58]. Here we present the results obtained for the fermionic machine, and note that the bosonic engine behaves equivalently. In Fig. 17 we plotted the concurrence (Fig. 17.a), CHSH values (Fig. 17.b) and singlet fractions (Fig. 17.c) for the fermionic thermal machine, as a function of Γ_φ.

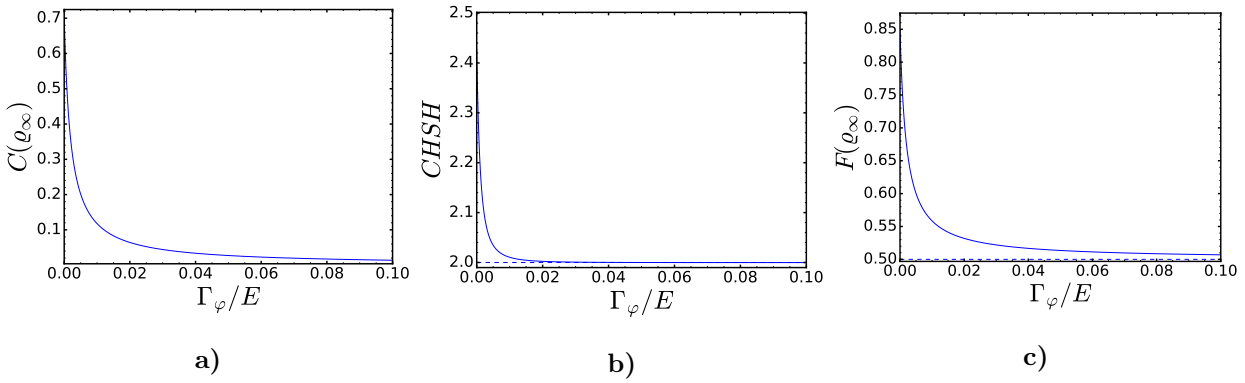

Figure 17: To study the robustness of the fermionic thermal machine against external decoherence, we plot here the different entanglement measures as function of external dephasing. Here we used $\Gamma_{\rm c}^-/E = 10^{-3}$; $\Gamma_{\rm h} = 100\Gamma_{\rm c}$; $T_c/E = 10^{-2}$; $T_h/E = 15$; $g/E = 3.5 \cdot 10^{-4}$.

The plots above illustrate that the dephasing decreases the amount of entanglement produced. When the strong Γ_φ limit is reached, the machines' systems are purified to the $|01\rangle$ (bosonic) or $|\mathrm{H}\rangle$ (fermionic) state. This occurs because the coherent dynamics are suppressed due to the strong decoherence of the off-diagonals, thus leaving the engines with an excitation incapable of escaping the hot bath-coupled qubit. Although the system is still capable of violating Bell's inequality, the system concurrence approaches zero, similarly to the discussion in Sec. 2.2.1. Overall, these findings shed light on the balance between entanglement generation of the described protocol and decoherence due to additional environments.

4.6 Transient Regime

In this section we study the transient regime in the evolution of each thermal machine. Our aim is to establish the required time scale to obtain the found steady state entanglement values, thereby determining the feasibility of experimentally implementing the presented protocol. To do so, we integrate the Lindblad equations derived in Sec. 3.4 and arrive at the expression $\hat{\varrho}_t = e^{\mathcal{L}_q t}\hat{\varrho}_0$ for $q \in \{\mathrm{F}, \mathrm{B}\}$, where $\hat{\varrho}_0$ corresponds to the initial condition of the system. Since we found the doubly excited state of each machine to exhibit an exponential decay profile in time (see Eq. (72) and Sec. 3.3), we initialize the system state as $\rho = (1/3, 1/3, 1/3, 0, 0, 0)$.

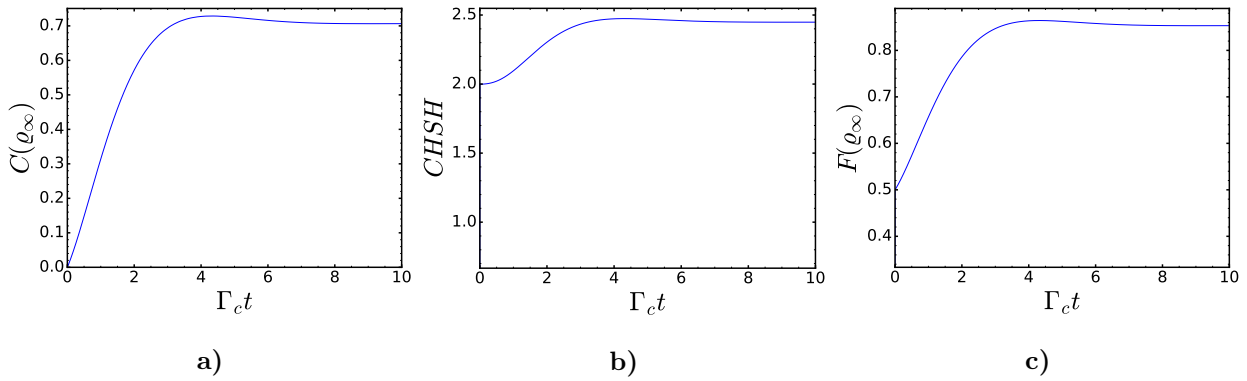

Figure 18: Here we plot concurrence (**a**), CHSH (**b**) and singlet fraction (**c**) over time for either thermal machine. The curves show how steady state entanglement is reached in a finite amount of time, using the initial condition $\rho = (1/3, 1/3, 1/3, 0, 0, 0)$. Here we used $\Gamma_c^-/E = 10^{-3}$; $\Gamma_h = 100\Gamma_c$; $T_c/E = 10^{-2}$; $T_h/E = 15$; $g/E = 3.5 \cdot 10^{-4}$; $dt = 0.05$.

Figure 18 illustrates the transient entanglement production of the bosonic thermal engine according to the concurrence (Fig. 18.a), CHSH value (Fig. 18.b) and singlet fraction (Fig. 18.c). The results obtained for the fermionic engine hold similar resemblance, thus we do not show them here. From Fig. 18 we note that the entanglement production over time according to each measure has very similar behaviours. More importantly, we note that the steady state entanglement values obtained in Sec. 4.1, 4.2 are achievable in a finite amount of time. Using the parameters chosen in this thesis the steady state would be reached in roughly 8000 s. However, note that this can be shortened by accurately choosing a higher Γ_c value. Lastly, we also note that our equations predict slightly higher entanglement values are achievable within the transient regime.

5 Conclusion and Outlook

In conclusion, we developed a continuous feedback control protocol capable of increasing the entanglement generation of the studied thermal engines. The developed protocol improves the concurrence generation by roughly three times in the fermionic engine, and roughly seven times in the bosonic case, compared to a feedback and measurement free evolution. Furthermore, in contrast to the results obtained in the absence of measurement and feedback, we show that the entanglement generated through the presented protocol is useful in an operational sense, as both engines are capable of quantum teleportation with relatively high fidelity, and violate Bell's inequality. In addition, we explored the robustness of the developed protocol under a series of different physical conditions. We determined that, independently of the engine, the hot bath must be at least 80% isolated, and any lower isolation value would render the generated entanglement useless. Furthermore, we studied the robustness of the generated entanglement against external decoherence. Here we found the systems to remain operationally useful at high coupling strengths with external environments, whilst assuming a faster detector response rate. Moreover, we studied the practicality of experimentally implementing either engine. This was done by verifying that the engines would require a finite amount of time to reach their steady state, roughly 8000 s, but note that lower times could be achieved by selecting a higher Γ_c value.

We have also provided a detailed discussion regarding effects of the presented implementation. We find that the protocol is capable of emulating the dynamics obtained by the presence of a strong repulsion term between the qubits of either engine. As we showed, this feature allows the bosonic engine to produce concurrence values that are equivalent to the ones produced by the fermionic engine. This is a distinctive result as, in the free evolution case, the fermionic engine was capable of greatly outperforming its bosonic counterpart. This difference is established by the presence of a repulsion term within the fermionic engine, which is however difficult to phenomenologically justify in the bosonic engine. In addition, the developed protocol is shown to establish a direct relation between the heat from the hot bath and the concurrence of either engine. This result suggests that the entanglement generated in an experimental setting through this feedback protocol could be determined without the use of quantum state tomography.

Overall, the investigation presented in this thesis opens the door to new possible explorations. Firstly, it has to be recognized that the limit of a detector faster than all other system dynamics is not achievable by most experimental settings. Through our equations it is clear that relaxing this limit cannot be but detrimental for the entanglement generation of either engine. However, an in depth study of the system dynamics in a slower detector limit is necessary in order to make predictions regarding the performance of the presented protocol in an experimental setting. Secondly, the derivation of a direct relation between concurrence and heat currents opens the doors to questions regarding entanglement witnesses and the energy cost for entanglement generation. It would be instructive to find a relation when simultaneously relaxing the limits of $\lambda \to \infty$ and $\gamma \gg \{g, \Gamma_c, \Gamma_h\}$. We believe that a deeper characterisation of the relation between heat and entanglement could allow for a better understanding of the entanglement generation properties of autonomous quantum thermal engines. Lastly, the presented protocol could be extended to more sophisticated engines. For instance, it could be interesting to relax the strong intra-dot repulsion in the

fermionic engine. This would allow for more than one fermion to exist in either dot. Through such exploration one could extend the present study to multipartite entanglement and study the effects of the protocol on more interesting systems in regards to quantum computation processes.

Appendices

A Completness of Weak Measurement Operators

In this section we show the derivation required to establish the completness relation $\int_{-\infty}^{\infty} \hat{W}^\dagger(z)\hat{W}(z)dz = 1$. Let us start by expanding for the expression of the weak measurement operators

$$\int_{-\infty}^{\infty} \hat{W}^\dagger(z)\hat{W}(z)dz = \left(\frac{2\kappa}{\pi}\right)^{\frac{1}{2}} \int_{-\infty}^{\infty} \left(e^{-\kappa\left(z-\hat{A}\right)^2}\right)^\dagger e^{-\kappa\left(z-\hat{A}\right)^2} dz \tag{77}$$

$$= \left(\frac{2\kappa}{\pi}\right)^{\frac{1}{2}} \int_{-\infty}^{\infty} e^{-2\kappa\left(z-\hat{A}\right)^2}. \tag{78}$$

To arrive at Eq. (78) we assumed the hermitianity of the operator $z-\hat{A}$, which for a suitable choice of $\hat{A}$ is easily ensured. The continuation of the derivation follows the standard approach taken in deriving the result of Gaussian integrals. We start by defining I as the expression of Eq. (78). We then perform a u-substitution, such that $x \equiv z - \hat{A} \Rightarrow dz = dx$. We then consider the integral I^2 instead and move to polar coordinates $r = \sqrt{x^2+y^2}$ and $\phi = \tan^{-1}(\frac{y}{x})$ as such

$$I^2 = \frac{2\kappa}{\pi} \int_{-\infty}^{\infty}\int_{-\infty}^{\infty} e^{-2\kappa(x+y)^2} dxdy \tag{79}$$

$$= \frac{2\kappa}{\pi} \int_0^{2\pi}\int_0^{\infty} e^{-2\kappa r^2} r dr d\phi \tag{80}$$

$$= \frac{1}{\pi}\int_0^{2\pi} \left[-\frac{1}{2}e^{-2\kappa r^2}\right]_0^{\infty} d\phi = 2\left[-\frac{1}{2}e^{-2\kappa r^2}\right]_0^{\infty} = 1 \tag{81}$$

$$\Rightarrow I = \sqrt{I^2} = 1. \tag{82}$$

B Transitions Involving the Doubly Occupied State

The Lindblad master equation for the free evolution of the fermionic system can be written as $\mathcal{L}_{\mathrm{F}}\hat{\varrho} = \mathcal{L}_{\mathrm{C}}\hat{\varrho} + \mathcal{L}_{\mathrm{H}}\hat{\varrho} + \mathcal{L}_{\mathrm{CH}}\hat{\varrho}$. In Sec. 3.3 we provided a full expression for the the terms $\mathcal{L}_{\mathrm{C}}$ and $\mathcal{L}_{\mathrm{H}}$, thereby showing their relation to the transition events due to interactions with the cold and hot bath respectively. On the other hand, $\mathcal{L}_{\mathrm{CH}}$ contains all information regarding the transitions involving the doubly occupied state $|\mathrm{CH}\rangle$

$$\begin{aligned}\mathcal{L}_{CH} =& \Gamma_{\mathrm{c}} n_{\mathrm{F}}(\varepsilon+U, T_{\mathrm{c}})\mathcal{D}[|\mathrm{CH}\rangle\langle\mathrm{H}] + \Gamma_{\mathrm{h}} n_{\mathrm{F}}(\varepsilon+U, T_{\mathrm{h}})\mathcal{D}[|\mathrm{CH}\rangle\langle\mathrm{C}] + \\ &+ \Gamma_{\mathrm{c}}(1-n_{\mathrm{F}}(\varepsilon+U, T_{\mathrm{c}}))\mathcal{D}[|\mathrm{H}\rangle\langle\mathrm{CH}] + \Gamma_{\mathrm{h}}(1-n_{\mathrm{F}}(\varepsilon+U, T_{\mathrm{h}}))\mathcal{D}[|\mathrm{C}\rangle\langle\mathrm{CH}],\end{aligned} \tag{83}$$

where $\mathcal{D}[\hat{O}]\hat{\varrho} \equiv \hat{O}\hat{\varrho}\hat{O}^\dagger - \frac{1}{2}\left\{\hat{O}^\dagger\hat{O}, \hat{\varrho}\right\}$ for any operator $\hat{O}$. In the limit $U \to \infty$, the system's dynamics are greately simplified. In this limit, the term $\mathcal{L}_{\mathrm{CH}}$ reduces to an equation which describes only transitions where the system abandons the doubly occupied state $|\mathrm{CH}\rangle$. Moreover, using Eq. (48) we obtain the equation of motion for the element $\hat{\varrho}_{\mathrm{CH}} \equiv \langle\mathrm{CH}|\hat{\varrho}|\mathrm{CH}\rangle$ to

be

$$\lim_{U\to\infty} \partial_t \hat{\varrho}_{\mathrm{CH}} = -(\Gamma_{\mathrm{h}} + \Gamma_{\mathrm{c}})\hat{\varrho}_{\mathrm{CH}}, \tag{84}$$

which has solution $\hat{\varrho}_{\mathrm{CH}} \approx e^{-(\Gamma_{\mathrm{c}}+\Gamma_{\mathrm{h}})t}$. These results suggests that, in the long time limit, the doubly occupied state is prohibited. This can be also qualitatively understood by considering that two strongly interacting electrons would repel eachother, thus limiting the number of dots that can be simultaneously occupied.

C Interpretation of Post-Measurement States

In this section, we present a brief discussion regarding the interpretation of post-measurement representations of mixed states.

Consider we were given a mixture of different pure states represented by the density operator $\hat{\varrho} = \sum_i p(i)|\phi_i\rangle\langle\phi_i|$. Now suppose that we wished to perform a measurement on the system via the measurement operator $\hat{M}_z$, where m corresponds to the measurement outcome for measuring $\hat{\varrho}$: the state of the system after such measure would be given by

$$\hat{\varrho}_z = \frac{\hat{M}_z\hat{\varrho}\hat{M}_z^\dagger}{\mathrm{Tr}\left\{\hat{M}_z\hat{\varrho}\hat{M}_z^\dagger\right\}} = \frac{\hat{M}_z\hat{\varrho}\hat{M}_z^\dagger}{p_z}, \tag{85}$$

where $p_z = \mathrm{Tr}\left\{\hat{M}_z\hat{\varrho}\hat{M}_z^\dagger\right\}$ corresponds to the probability of obtaining outcome z and serves the purpose to normalize the state $\hat{\varrho}_z$, as required by Eq. (7). By expanding Eq. (85) into the outerproduct of the state vectors of the system, we can use Bayes theorem to write

$$\hat{\varrho}_z = \sum_i \frac{p(i)}{p_z}\hat{M}_z|\phi_i\rangle\langle\phi_i|\hat{M}_z^\dagger \tag{86}$$

$$= \sum_i \frac{p(i)}{p_z}p(m|i)|\phi_i^m\rangle\langle\phi_i^m| \tag{87}$$

$$= \sum_i p(i|z)|\phi_i^z\rangle\langle\phi_i^z|. \tag{88}$$

In the above equations we have defined $|\phi_i^z\rangle \equiv \frac{\hat{M}_z|\phi_i\rangle}{\sqrt{p(z|i)}}$ as the post measurement representation of the state vector $|\phi_i\rangle$. Given the result obtained in Eq. (88) we define $\hat{\varrho}_z$ as a conditional (selective) state: i.e. the state of the system given z was measured. Let us now consider the case in which we do not normalize $\hat{\varrho}_z$, such that $\hat{\varrho}' \equiv p_z\hat{\varrho}_z$. In this case we can use Eq. (87) together with some probability theory to write

$$\hat{\varrho}' = \sum_i p(z,i)|\phi_i^z\rangle\langle\phi_i^z|. \tag{89}$$

The equation expressed above can be interpreted as representing the joint state of system and outcome: similar expressions are referred to as non-selective states. Non-selective states are interpreted as systems that have been measured, but whose outcome has been ignored.

In this thesis we have encountered both conditional and non-selective states. As an example, Eq. (33) is a conditional state, as the final expression for $\hat{\varrho}$ is dependent on the measurement outcome D. On the other hand, Eq. (68) is a clear example of non-selective state. One could, in theory, start from the conditional state in Eq. (33) and arrive at a non selective steady state by repeatedly applying the measurement superoperators $\mathscr{M}(z)$ and $\mathcal{L}$ such that

$$\hat{\varrho}_{t_f}(\overline{z}) = e^{\mathcal{L}dt}\mathscr{M}(z_n)...e^{\mathcal{L}dt}\mathscr{M}(z_1)\hat{\varrho}(0). \tag{90}$$

The final expression obtained by the above procedure is defined as a "trajectory". By averaging over several of these trajectories we get rid of the measurement outcome dependency, such that we obtain the non selective steady state

$$\hat{\varrho}_{t_f} = \int_{-\infty}^{\infty} \hat{\varrho}_{t_f}(\overline{z})d\overline{z} \tag{91}$$

D Master Equation for Measurement Backaction

In this section, we derive a differential equation to describe the measurement backaction on a system freely evolving according to Eq. (14). We start by dividing time into discrete steps of duration dt. We then, iteratively measure the system and let it evolve. Thus, at time $t + dt$ the system is in state

$$\hat{\varrho}_{t+dt}(z) = e^{\mathcal{L}dt}\mathcal{M}(z)\hat{\varrho}(t). \tag{92}$$

In the above, we defined $\mathcal{M}(z)\hat{\varrho} = \hat{K}(z)\hat{\varrho}\hat{K}^{\dagger}(z)$ and $\mathcal{L}\hat{\varrho}$ as the superoperator representations for the measurement and time evolution (see Eq. (14),(29)) operations. In order to obtain an expression for the non-selective state representation, we integrate Eq. (92) over all possible outcomes z

$$\hat{\varrho}_{t+dt} = e^{\mathcal{L}dt}\int_{-\infty}^{\infty} dz\mathcal{M}(z)\hat{\varrho}(t) \tag{93}$$

$$= e^{\mathcal{L}dt}\left(\frac{2\lambda dt}{\pi}\right)^{1/2}\int_{-\infty}^{\infty} dz e^{-\lambda dt\left(z-\hat{A}\right)^2}\hat{\varrho}(t)e^{-\lambda dt\left(z-\hat{A}\right)^2} \tag{94}$$

$$= e^{\mathcal{L}dt}\left(\frac{2\lambda dt}{\pi}\right)^{1/2}\int_{-\infty}^{\infty} dz \sum_{ij} e^{-\lambda dt\left[(z-A_i)^2+(z-A_j)^2\right]}|a_i\rangle\langle a_i|\hat{\varrho}(t)|a_j\rangle\langle a_j|. \tag{95}$$

To arrive at the last equality in the above derivation, we have inserted the completeness relation $\mathbb{1} = \sum_i |a_i\rangle\langle a_i|$ twice. The orthonormal states $|a_i\rangle$ are chosen as the eigenstates of the observable $\hat{A}$ with eigenvalue A_i (i.e. $\hat{A}|a_i\rangle = A_i|a_i\rangle$). Computing the integral in Eq. (95) leads to

$$\hat{\varrho}(t+dt) = e^{\mathcal{L}dt}\sum_{ij} e^{-\lambda dt(-A_iA_j+\frac{1}{2}A_i^2+\frac{1}{2}A_j^2)}|a_i\rangle\langle a_i|\hat{\varrho}(t)|a_j\rangle\langle a_j| \tag{96}$$

$$\approx (1+\mathcal{L}dt)\sum_{ij}\left[1-\lambda dt\left(-A_iA_j+\frac{1}{2}A_i^2+\frac{1}{2}A_j^2\right)\right]|a_i\rangle\langle a_i|\hat{\varrho}(t)|a_j\rangle\langle a_j| \tag{97}$$

$$= \hat{\varrho}(t) + dt\mathcal{L}\hat{\varrho}(t) + \lambda dt\left(\hat{A}\hat{\varrho}(t)\hat{A} - \frac{1}{2}\left\{\hat{A}^2, \hat{\varrho}(t)\right\}\right). \tag{98}$$

In the second line of the above derivation we have expanded the exponential term up to first order in dt. This approximation is not to be considered detrimental for the derivation, as, in the next step, we consider the continuous limit $dt \to 0$. In this limit we use the definition of a derivative to write the final expression for the master equation

$$\frac{d\hat{\varrho}(t)}{dt} = \mathcal{L}\hat{\varrho}(t) + \lambda \mathcal{D}[\hat{A}]\hat{\varrho}(t), \tag{99}$$

where we introduced the superoperator $\mathcal{D}[\hat{A}]\hat{\varrho} = \hat{A}\hat{\varrho}\hat{A} - \frac{1}{2}\left\{\hat{A}^2, \hat{\varrho}\right\}$ to represent the measurement backaction. Equation (99) is similar to Eq. (14) with the addition of an extra term proportional to the measurement strength λ. The additional term represents the measurement backaction, and it has the effect of adding a dampening term to the coherences of $\hat{\varrho}$.

Briefly, we now show that in the limit $dt \to 0$ we obtain the commutation relation $e^{\mathcal{L}dt}\mathcal{M}(z)\hat{\varrho} = \mathcal{M}(z)e^{\mathcal{L}dt}\hat{\varrho}$. To do so, we derive master equation (99) starting from the differential increment $\hat{\varrho}_{t+dt}(z) = \mathcal{M}(z)e^{\mathcal{L}dt}\hat{\varrho}$ instead. By following the steps used to derive Eq. (99), we arrive at the expression

$$\frac{\hat{\varrho}(t+dt) - \hat{\varrho}(t)}{dt} = \mathcal{L}\hat{\varrho}(t) + \lambda\left(\hat{A}\hat{\varrho}(t)\hat{A} - \frac{1}{2}\left\{\hat{A}^2, \hat{\varrho}(t)\right\}\right) + \lambda dt\left(\hat{A}\mathcal{L}\hat{\varrho}(t)\hat{A} - \frac{1}{2}\left\{\hat{A}^2, \mathcal{L}\hat{\varrho}(t)\right\}\right), \tag{100}$$

in the limit $dt \to 0$ the third term on the right-hand side of the above relation vanishes, while the left-hand side approaches the definition of a derivative, leaving us with Eq. (99).

E Filtering

When measuring an arbritrary observable of a system, we use the parameter $z(t)$ to label the measurement outcomes. The use of Eq. (30) leads to the variance of z to diverge in the continuous limit $\Delta t \to 0$, as

$$\mathrm{Var}[z(t)] = \frac{1}{4\lambda\Delta t}. \tag{101}$$

This implies that in the continuous limit, the information extracted in the form of $z(t)$ will serve no use. To show this, we ran a Monte Carlo simulation for the time evolution of a continuously monitored system, where we set Δt to be the system smallest parameter. The simulation was made so that it would return a conditional state , starting from a system initialized in $\hat{\varrho}_i = |10\rangle\langle 10|$ state. The results shown in Fig. 3 show how $z(t)$ does not provide any useful information, as its fast oscillatory behaviour and high variance, make it impossible to distinguish the state of the system at any given time. To obtain any useful information we need to process the measurement outcomes. In order to clean the outcomes $z(t)$ we need to filter out the higher frequency behaviour of the signal. To do so we make use of the convolution in Eq. (34). To obtain the results obtained in Fig. 3 we used Eq. (34), to derive a Markovian update equation

$$D(t+dt) = D(t) + \gamma dt[z(t) - D(t)] \tag{102}$$

Though seemingly arbitrary, the convolution in Eq. (34) behaves as a low pass filter by removing all fast oscillatory behaviours and outputting a signal with time independent variance (see rightmost plot in Fig. 3)

$$\mathrm{Var}[D(t)] = \frac{\gamma}{8\lambda}. \tag{103}$$

We can convince ourselves of the filtering properties of Eq. (34) by studying its spectral density function. That is, if we consider the Fourier transform of Eq. (34), we find it to be the product of the signal $z(t)$, in Fourier space, and a Lorentzian function centered at the origin (note that $t \geq 0$ and thus we can write $t \to |t|$). From this, it is clear that $D(t)$ contains only low valued frequency components of $z(t)$, as the higher frequency components are filtered out by the rapidly decaying tail of the Lorentzian function obtained through the Fourier transform of the exponential term.

F Analytical Treatment of Free Evolution Scenario

In this section we study in more detail the free evolution of the fermionic thermal engine. Note that an analogous treatment of the free evolution of the bosonic engine can be made using the same techniques presented in this section. For the ease of the reader, we here restate the details needed to reconstruct the dynamics of the fermionic engine. Using the occupation number basis, the system's Hamiltonian is

$$\hat{H} = \varepsilon\left(|\mathrm{C}\rangle\langle\mathrm{C}| + |\mathrm{H}\rangle\langle\mathrm{H}|\right) + g\left(|\mathrm{C}\rangle\langle\mathrm{H}| + \mathrm{h.c.}\right) + (2\varepsilon + U)\,|\mathrm{CH}\rangle\langle\mathrm{CH}|, \tag{104}$$

where the term U represents the interdot Coulomb interaction energy. Due to the coupling to the thermal environments, the system dynamics are described by the Lindblad equation

$$\partial_t \hat{\varrho}_t = -i\left[\hat{\mathrm{H}}, \hat{\varrho}_t\right] + \sum_{j=\mathrm{C,H}} \left(\Gamma_j^+ \mathcal{D}[|j\rangle\langle 0|] + \Gamma_j^- \mathcal{D}[|0\rangle\langle j|]\right) + \mathcal{L}_{\mathrm{CH}}, \tag{105}$$

where the tunneling probabilities are given by $\Gamma_j^+ \equiv \Gamma_j n_{\mathrm{F}}(\varepsilon, T_j)$ and $\Gamma_j^- \equiv \Gamma_j(1 - n_{\mathrm{F}}(\varepsilon, T_j))$, where $n_{\mathrm{F}}(\varepsilon, T) \equiv \frac{1}{e^{(\varepsilon-\mu)/T}+1}$ is the Fermi-Dirac distribution (note $k_b \equiv 1$) and Γ_j is the coupling strength to bath j. Lastly, the term $\mathcal{L}_{\mathrm{CH}}$ contains all information regarding the transitions involving the doubly occupied state $|\mathrm{CH}\rangle$ (see appendix B). Note that we here consider the limit case $U \to \infty$, which allows us to safely discard the $\mathcal{L}_{\mathrm{CH}}$, as the $|\mathrm{CH}\rangle$ state is prohibited.

As Eq. (105) is linear in the system's state $\hat{\varrho}$, it can be rewritten in a matrix-vector multiplication fashion, by unwrapping $\hat{\varrho}$ into a vector ρ_t, such that $\rho \equiv (\langle 0|\hat{\varrho}|0\rangle, \langle \mathrm{C}|\hat{\varrho}|\mathrm{C}\rangle, \langle \mathrm{H}|\hat{\varrho}|\mathrm{H}\rangle, \alpha, \alpha^*)^T$ where $\alpha \equiv \langle \mathrm{C}|\hat{\varrho}|\mathrm{H}\rangle$, leading to the differential equation $\partial_t \rho_t = \mathscr{L}_{\mathrm{F}} \rho_t$. The superoperator $\mathscr{L}_{\mathrm{F}}$ is then written as a 5×5 matrix with form

$$\mathscr{L}_{\mathrm{F}} = \begin{bmatrix} -\Gamma_{\mathrm{c}}^+ - \Gamma_{\mathrm{h}}^+ & \Gamma_{\mathrm{c}}^- & \Gamma_{\mathrm{h}}^- & 0 & 0 \\ \Gamma_{\mathrm{c}}^+ & -\Gamma_{\mathrm{c}}^- & 0 & ig & -ig \\ \Gamma_{\mathrm{h}}^+ & 0 & -\Gamma_{\mathrm{h}}^- & -ig & ig \\ 0 & ig & -ig & -\frac{1}{2}\left(\Gamma_{\mathrm{c}}^- + \Gamma_{\mathrm{h}}^-\right) & 0 \\ 0 & -ig & ig & 0 & -\frac{1}{2}\left(\Gamma_{\mathrm{c}}^- + \Gamma_{\mathrm{h}}^-\right) \end{bmatrix}. \tag{106}$$

The steady state $\hat{\varrho}_\infty$ is then given by the eigenvector ρ_∞ of $\mathscr{L}_\mathrm{F}$ whose eigenvalue is zero (i.e. the null-space of $\mathscr{L}_\mathrm{F}$), as $\partial_t\hat{\varrho}_\infty = \mathscr{L}_\mathrm{F}\hat{\varrho}_\infty = 0$. Thus, by calculating the kernel of Eq. (106) we find

$$\begin{aligned}\hat{\varrho}_\infty = \frac{1}{\mathcal{N}}\big[&\left(\Gamma_\mathrm{c}^- + \Gamma_\mathrm{h}^-\right)\left(4g^2 + \Gamma_\mathrm{c}^-\Gamma_\mathrm{h}^-\right)|0\rangle\langle 0| + \left(\Gamma_\mathrm{c}^+\Gamma_\mathrm{h}^-(\Gamma_\mathrm{c}^- + \Gamma_\mathrm{h}^-) + 4g^2(\Gamma_\mathrm{c}^+ + \Gamma_\mathrm{h}^+)\right)|\mathrm{C}\rangle\langle\mathrm{C}| + \\ &+ \left(\Gamma_\mathrm{c}^-\Gamma_\mathrm{h}^+(\Gamma_\mathrm{c}^- + \Gamma_\mathrm{h}^-) + 4g^2(\Gamma_\mathrm{c}^+ + \Gamma_\mathrm{h}^+)\right)|\mathrm{H}\rangle\langle\mathrm{H}| + 2ig\left(\Gamma_\mathrm{c}^-\Gamma_\mathrm{h}^+ - \Gamma_\mathrm{c}^+\Gamma_\mathrm{h}^-\right)\left(|\mathrm{H}\rangle\langle\mathrm{C}| - |\mathrm{C}\rangle\langle\mathrm{H}|\right)\big], \quad (107)\end{aligned}$$

where $\mathcal{N} \equiv \left(\Gamma_\mathrm{c}^- + \Gamma_\mathrm{h}^-\right)\left(4g^2 + \Gamma_\mathrm{c}^-\Gamma_\mathrm{h}^- + \Gamma_\mathrm{c}^-\Gamma_\mathrm{h}^+ + \Gamma_\mathrm{c}^+\Gamma_\mathrm{h}^-\right) + 8g^2(\Gamma_\mathrm{c}^+ + \Gamma_\mathrm{h}^+)$ is a normalization factor. Optimal parameters for mamimal concurrence of Eq. (107) are then obtainable analytically by solving the differential equations $\nabla C(\hat{\varrho}_\infty) = 0$, or numerically through methods such as simulated annealing. Upon doing so, one would find an optimal value of $C(\hat{\varrho}_\infty) \sim 0.25$, however, the state $\hat{\varrho}_\infty$ obtained this way would not be able to violate Bell's inequality nor reproduce quantum teleportation.

G The Relation Between Heat and Entanglement

In this section we derive Eq. (73). In Sec. 2.3 we established that the change in energy within our systems is defined as $\dot{E} = \mathrm{Tr}\left\{\hat{H}\partial_t\hat{\varrho}\right\}$. In the limit of a fast detector, we replace $\partial_t\hat{\varrho}_t = \mathcal{L}(D)\hat{\varrho}_t(D)$ and separate the Lindblad operator into the terms concerning the interaction with the two baths (i.e. $\mathcal{L}_\mathrm{c}$ and $\mathcal{L}_\mathrm{h}$). To obtain a result for non-selective states we then integrate over all outcomes D

$$\begin{aligned}\dot{E} &= \mathrm{Tr}\left\{\hat{H}\partial_t\hat{\varrho}\right\} && (108)\\ &= \int_{-\infty}^{\infty} dD\,\mathrm{Tr}\left\{\hat{H}\mathcal{L}(D)\hat{\varrho}(D)\right\}\rangle && (109)\\ &= \int_{-\infty}^{\infty} dD\left([1-\theta(D)]\,\mathrm{Tr}\left\{\hat{H}\mathcal{L}_\mathrm{c}\hat{\varrho}(D)\right\} + \theta(D)\left(\mathrm{Tr}\left\{\hat{H}\mathcal{L}_\mathrm{c}\hat{\varrho}(D)\right\} + \mathrm{Tr}\left\{\hat{H}\mathcal{L}_\mathrm{h}\hat{\varrho}(D)\right\}\right)\right) && (110)\\ &= \mathrm{Tr}\left\{(\hat{H} - \mu_\mathrm{c}N)\mathcal{L}_\mathrm{c}\hat{\varrho}\right\} + \mathrm{Tr}\left\{(\hat{H} - \mu_\mathrm{h}N)\mathcal{L}_\mathrm{h}\mathcal{O}\hat{\varrho}\right\} + \mu_\mathrm{c}I_\mathrm{c} + \mu_\mathrm{h}I_\mathrm{h} && (111)\\ &= \dot{Q}_\mathrm{c} + \dot{Q}_\mathrm{h} + \mu_\mathrm{c}I_\mathrm{c} + \mu_\mathrm{h}I_\mathrm{h} && (112)\end{aligned}$$

In the above we have separated the heat into a component representing the thermal heat current $\dot{Q}_\nu$ and into a component representing the heat arising from the particle heat current I_ν. In the limiting cases of $T_\mathrm{c} \to 0$ and $\lambda \to \infty$ we use the steady state results derived in Sec. 4.1 to write the expression for the steady state heat currents

$$\dot{Q}_\mathrm{c} = -\frac{g^2\varepsilon\Gamma_\mathrm{c}\Gamma_\mathrm{h}^+}{g^2\left(\Gamma_\mathrm{c} + 2\Gamma_\mathrm{h}^+\right) + \frac{1}{4}\Gamma_\mathrm{c}^2\Gamma_\mathrm{h}^+}, \qquad \dot{Q}_\mathrm{h} = \frac{g^2\varepsilon\Gamma_\mathrm{c}\Gamma_\mathrm{h}^+}{g^2\left(\Gamma_\mathrm{c} + 2\Gamma_\mathrm{h}^+\right) + \frac{1}{4}\Gamma_\mathrm{c}^2\Gamma_\mathrm{h}^+}. \quad (113)$$

As a first check we note that the above expressions return the expected result $Q = Q_\mathrm{c} + Q_\mathrm{h} = 0$. Furthermore we note that we can use the above expression to write the system concurrence in Eq. (113) as a function of the heat current $C_\mathrm{F}(\hat{\varrho}_\infty) = Q_\mathrm{h}/g\varepsilon$. An analogous derivation can be made for the bosonic system, which then recovers the relation $C_\mathrm{B}(\hat{\varrho}_\infty) = Q_\mathrm{h}/gE$.

Upon relaxing the $\lambda \to \infty$ condition, one finds the heat current from the hot bath to be

$$Q_{\mathrm{h}} = \frac{g^2(1-\eta)\varepsilon\Gamma_{\mathrm{c}}\Gamma_{\mathrm{h}}^{+}}{-\Gamma_{\mathrm{c}}\left(-g^2 - \frac{1}{4}\eta^2\left(\Gamma_{\mathrm{h}}^{-}\right)^2\right) + (1-\eta)\Gamma_{\mathrm{h}}^{+}\left(\frac{\Gamma_{\mathrm{c}}^2}{4} + \frac{1}{4}\eta\Gamma_{\mathrm{c}}\Gamma_{\mathrm{h}}^{-} + 2g^2\right) + \frac{1}{4}\eta\Gamma_{\mathrm{c}}^2\Gamma_{\mathrm{h}}^{-} + \eta g^2\Gamma_{\mathrm{h}}^{-}}, \tag{114}$$

which one can show to be related to the system concurrence as $C_{\mathrm{F}}(\hat{\varrho}_\infty) = Q_{\mathrm{h}}/g\varepsilon$. However, the same is not true in the bosonic case.

References

[1] J. B. Brask, G. Haack, N. Brunner, and M. Huber, "Autonomous quantum thermal machine for generating steady-state entanglement," *New Journal of Physics*, vol. 17, no. 11, p. 113029, nov 2015.

[2] R. Horodecki, P. Horodecki, M. Horodecki, and K. Horodecki, "Quantum entanglement," *Reviews of Modern Physics*, vol. 81, no. 2, pp. 865–942, jun 2009.

[3] D. Paneru, E. Cohen, R. Fickler, R. W. Boyd, and E. Karimi, "Entanglement: Quantum or classical?" *Reports on Progress in Physics*, vol. 83, no. 6, p. 064001, 2020.

[4] F. Dupuis, O. Fawzi, and S. Wehner, "Entanglement sampling and applications," *IEEE Transactions on Information Theory*, vol. 61, no. 2, pp. 1093–1112, feb 2015.

[5] N. Zou, "Quantum entanglement and its application in quantum communication," *Journal of Physics: Conference Series*, vol. 1827, no. 1, p. 012120, 2021.

[6] P. Shor, "Algorithms for quantum computation: discrete logarithms and factoring," in *Proceedings 35th Annual Symposium on Foundations of Computer Science*, 1994, pp. 124–134.

[7] D. Coppersmith, "An approximate fourier transform useful in quantum factoring," 2002.

[8] H.-L. Shi, S. Ding, Q.-K. Wan, X.-H. Wang, and W.-L. Yang, "Entanglement, coherence, and extractable work in quantum batteries," *Phys. Rev. Lett.*, vol. 129, p. 130602, Sep 2022.

[9] M. Perarnau-Llobet, K. V. Hovhannisyan, M. Huber, P. Skrzypczyk, N. Brunner, and A. Acín, "Extractable work from correlations," *Phys. Rev. X*, vol. 5, p. 041011, Oct 2015.

[10] H.-P. Breuer and F. Petruccione, *The theory of Open Quantum Systems*. Clarendon, 2010.

[11] M. A. Nielsen and I. L. Chuang.

[12] J. Wang, H. M. Wiseman, and G. J. Milburn, "Dynamical creation of entanglement by homodyne-mediated feedback," *Phys. Rev. A*, vol. 71, p. 042309, Apr 2005.

[13] A. R. R. Carvalho and J. J. Hope, "Stabilizing entanglement by quantum-jump-based feedback," *Phys. Rev. A*, vol. 76, p. 010301, Jul 2007.

[14] A. R. R. Carvalho, A. J. S. Reid, and J. J. Hope, "Controlling entanglement by direct quantum feedback," *Phys. Rev. A*, vol. 78, p. 012334, Jul 2008.

[15] M. B. Plenio, S. F. Huelga, A. Beige, and P. L. Knight, "Cavity-loss-induced generation of entangled atoms," *Phys. Rev. A*, vol. 59, pp. 2468–2475, Mar 1999.

[16] M. S. Kim, J. Lee, D. Ahn, and P. L. Knight, "Entanglement induced by a single-mode heat environment," *Phys. Rev. A*, vol. 65, p. 040101, Apr 2002.

[17] F. Benatti, R. Floreanini, and M. Piani, "Environment induced entanglement in markovian dissipative dynamics," *Phys. Rev. Lett.*, vol. 91, p. 070402, Aug 2003.

[18] J. Bohr Brask, F. Clivaz, G. Haack, and A. Tavakoli, "Operational nonclassicality in minimal autonomous thermal machines," *Quantum*, vol. 6, p. 672, 2022.

[19] G. Maslennikov, S. Ding, R. Hablützel, J. Gan, A. Roulet, S. Nimmrichter, J. Dai, V. Scarani, and D. Matsukevich, "Quantum absorption refrigerator with trapped ions," *Nature Communications*, vol. 10, no. 1, 2019.

[20] J. Roßnagel, S. T. Dawkins, K. N. Tolazzi, O. Abah, E. Lutz, F. Schmidt-Kaler, and K. Singer, "A single-atom heat engine," *Science*, vol. 352, no. 6283, p. 325–329, 2016.

[21] M. H. M. Passos, A. C. Santos, M. S. Sarandy, and J. A. O. Huguenin, "Optical simulation of a quantum thermal machine," *Phys. Rev. A*, vol. 100, p. 022113, Aug 2019.

[22] B. Leggio, B. Bellomo, and M. Antezza, "Quantum thermal machines with single nonequilibrium environments," *Physical Review A*, vol. 91, no. 1, 2015.

[23] P. P. Hofer, J.-R. Souquet, and A. A. Clerk, "Quantum heat engine based on photon-assisted cooper pair tunneling," *Phys. Rev. B*, vol. 93, p. 041418, Jan 2016.

[24] N. Linden, S. Popescu, and P. Skrzypczyk, "The smallest possible heat engines," 2010.

[25] K. Jacobs and D. A. Steck, "A straightforward introduction to continuous quantum measurement," *Contemporary Physics*, vol. 47, no. 5, pp. 279–303, sep 2006.

[26] D. Manzano, "A short introduction to the lindblad master equation," *AIP Advances*, vol. 10, no. 2, p. 025106, feb 2020.

[27] L. Miš ta and R. Tatham, "Gaussian intrinsic entanglement: An entanglement quantifier based on secret correlations," *Physical Review A*, vol. 91, no. 6, jun 2015.

[28] J. Um, H. Park, and H. Hinrichsen, "Entanglement versus mutual information in quantum spin chains," *Journal of Statistical Mechanics: Theory and Experiment*, vol. 2012, no. 10, 2012.

[29] M. B. Plenio, "Logarithmic negativity: A full entanglement monotone that is not convex," *Physical Review Letters*, vol. 95, no. 9, aug 2005.

[30] W. K. Wootters, "Entanglement of formation of an arbitrary state of two qubits," *Physical Review Letters*, vol. 80, no. 10, p. 2245–2248, 1998.

[31] S. Virmani and M. Plenio, "Ordering states with entanglement measures," *Physics Letters A*, vol. 268, no. 1-2, p. 31–34, 2000.

[32] C. H. Bennett, G. Brassard, C. Crépeau, R. Jozsa, A. Peres, and W. K. Wootters, "Teleporting an unknown quantum state via dual classical and einstein-podolsky-rosen channels," *Phys. Rev. Lett.*, vol. 70, pp. 1895–1899, Mar 1993.

[33] S. Popescu, "Bell's inequalities versus teleportation: What is nonlocality?" *Physical Review Letters*, vol. 72, no. 6, p. 797–799, 1994.

[34] M. Horodecki, P. Horodecki, and R. Horodecki, "General teleportation channel, singlet fraction, and quasidistillation," *Physical Review A*, vol. 60, no. 3, p. 1888–1898, 1999.

[35] "Can quantum-mechanical description of physical reality be considered complete?" vol. 47.

[36] "On the einstein podolsky rosen paradox."

[37] "Publisher correction: Challenging local realism with human choices," *Nature*, vol. 562, no. 7727, 2018.

[38] D. Rauch, J. Handsteiner, A. Hochrainer, J. Gallicchio, A. S. Friedman, C. Leung, B. Liu, L. Bulla, S. Ecker, F. Steinlechner, and et al., "Cosmic bell test using random measurement settings from high-redshift quasars," *Physical Review Letters*, vol. 121, no. 8, 2018.

[39] D. A. Redman, S. Brown, R. H. Sands, and S. C. Rand, "Spin dynamics and electronic states of n-vcenters in diamond by epr and four-wave-mixing spectroscopy," *Physical Review Letters*, vol. 67, no. 24, p. 3420–3423, 1991.

[40] "Proposed experiment to test local hidden-variable theories," vol. 23.

[41] R. Horodecki, P. Horodecki, and M. Horodecki, "Violating bell inequality by mixed states: Necessary and sufficient condition," *Physics Letters A*, vol. 200, no. 5, p. 340–344, 1995.

[42] S. Khandelwal, N. Palazzo, N. Brunner, and G. Haack, "Critical heat current for operating an entanglement engine," *New Journal of Physics*, vol. 22, no. 7, p. 073039, jul 2020.

[43] P. P. Potts, A. A. S. Kalaee, and A. Wacker, "A thermodynamically consistent markovian master equation beyond the secular approximation," *New Journal of Physics*, vol. 23, no. 12, p. 123013, dec 2021.

[44] G. Schaller, *Open quantum systems far from equilibrium*, 2016.

[45] P. A. Mello, "The von neumann model of measurement in quantum mechanics," in *AIP Conference Proceedings*. AIP Publishing LLC, 2014.

[46] A. Bednorz, W. Belzig, and A. Nitzan, "Nonclassical time correlation functions in continuous quantum measurement," *New Journal of Physics*, vol. 14, no. 1, p. 013009, 2012.

[47] S. Becker, N. Datta, and R. Salzmann, "Quantum zeno effect in open quantum systems," *Annales Henri Poincaré*, vol. 22, no. 11, p. 3795–3840, 2021.

[48] T. Möbus and M. M. Wolf, "Quantum zeno effect generalized," *Journal of Mathematical Physics*, vol. 60, no. 5, p. 052201, 2019.

[49] D. Barker, M. Scandi, S. Lehmann, C. Thelander, K. A. Dick, M. Perarnau-Llobet, and V. F. Maisi, "Experimental verification of the work fluctuation-dissipation relation for information-to-work conversion," *Phys. Rev. Lett.*, vol. 128, p. 040602, Jan 2022.

[50] S. J. Weber, A. Chantasri, J. Dressel, A. N. Jordan, K. W. Murch, and I. Siddiqi, "Mapping the optimal route between two quantum states," *Nature*, vol. 511, no. 7511, p. 570–573, 2014.

[51] K. W. Murch, S. J. Weber, C. Macklin, and I. Siddiqi, "Observing single quantum trajectories of a superconducting quantum bit," *Nature*, vol. 502, no. 7470, p. 211–214, 2013.

[52] Jacobs, *Quantum measurement theory and its applications*. Cambridge University Press, 2014.

[53] H. M. Wiseman, "Quantum theory of continuous feedback," *Phys. Rev. A*, vol. 49, pp. 2133–2150, Mar 1994.

[54] B. Annby-Andersson, F. Bakhshinezhad, D. Bhattacharyya, G. D. Sousa, C. Jarzynski, P. Samuelsson, and P. P. Potts, "Quantum fokker-planck master equation for continuous feedback control," *Physical Review Letters*, vol. 129, no. 5, jul 2022.

[55] D. Ristè, M. Dukalski, C. A. Watson, G. de Lange, M. J. Tiggelman, Y. M. Blanter, K. W. Lehnert, R. N. Schouten, and L. DiCarlo, "Deterministic entanglement of superconducting qubits by parity measurement and feedback," *Nature*, vol. 502, no. 7471, p. 350–354, 2013.

[56] W. P. Livingston, M. S. Blok, E. Flurin, J. Dressel, A. N. Jordan, and I. Siddiqi, "Experimental demonstration of continuous quantum error correction," *Nature Communications*, vol. 13, no. 1, 2022.

[57] K. Prech, P. Johansson, E. Nyholm, G. T. Landi, C. Verdozzi, P. Samuelsson, and P. P. Potts, "Entanglement and thermo-kinetic uncertainty relations in coherent mesoscopic transport," 2022.

[58] S. A. Gurvitz, "Measurements with a noninvasive detector and dephasing mechanism," *Phys. Rev. B*, vol. 56, pp. 15 215–15 223, Dec 1997.